UNIVERSITÀ DEGLI STUDI DI PADOVA
DIPARTIMENTO DI INGEGNERIA INDUSTRIALE

Corso di Laurea Magistrale in Materials Engineering

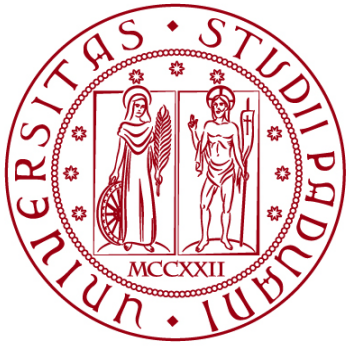

TESI DI LAUREA

"Structured Na_2SO_4 components and thermal properties of the Li_2SO_4-Na_2SO_4 system"

Relatore:
Prof.ssa Giorgia Franchin
Co-relatore:
Dr. Ali Ezzine

Laureando: Francesca Velludo
Matricola 2072758

ANNO ACCADEMICO 2023-2024

Abstract

The salts analysed are Li_2SO_4 and Na_2SO_4, what is relevant is the Li_2SO_4-Na_2SO4 system which is suitable for thermal energy storage due to a solid-solid phase transition that takes place at temperatures comprised between 475°C and 578°C. The temperature of the phase transition is related to the molar composition of the system.

By thermally treating tablets with different ratio of Na_2SO_4 and Li_2SO_4 it was possible to assess the accuracy of the phase diagram and to detect the reason of the change in colour of the tablets when treated at temperatures above 500°C.

Additive manufacturing, specifically direct ink writing, was used to produce Na_2SO_4 components in order to detect the mechanical properties of different geometries with different percentages of porosity.

The aforementioned technique is used to obtain 3D structures with customizable geometries that in this case were designed in order to allow volume changes that occur during the phase transitions.

In order to extrude the salt an ink made of Na_2SO_4, Ehtanol and Polyvinylpyrrolidone was produced.

Contents

Chapter 1 - Introduction

1.1 Phase Change materials

Phase Change Materials (PCM) are substances that can absorb or release latent heat when they go through a change in their physical state. The phase change typically occurs between two states of matter but it could also involve a phase modulation between two intermediate crystalline structures each with a different energy level.

By melting, solidifying or changing the crystalline structure at the phase-change temperature a PCM is able to store and release large amounts of energy as latent heat (energy that is transferred in a process, without a change in temperature of the body as opposed to sensible heat which is energy exchanged with a consequent change in the temperature of the body).

The PCM can be classified as:

- organic PCM, they are subdivided into Paraffins and non-Paraffins compounds, they possess a high heat of fusion, they are chemically stable and they are non-toxic. The disadvantages are the high flammability, the low volumetric latent heat storage and the low thermal conductivity.
- inorganic PCM, they can be divided into salt hydrate and metallic hydrate, they are characterized by wide availability, low costs, high latent heat storage capacity, sharp melting point, generally low volume change, high thermal conductivity and high heat of fusion. The disadvantages are related to corrosion of other materials, incongruent melting, phase separation during cycling and high volume change in certain mixtures [1].
- eutectic PCM, they consist of a combination of two types of PCMs: organic-organic, inorganic-inorganic, or organic-inorganic. In these materials, all components melt simultaneously into a liquid state and crystallize together during the cooling process. Typically, eutectic water-salt solutions are employed for energy storage at temperatures below 0 degrees Celsius.

1.2 Additive manufacturing

Additive Manufacturing (AM), also known as 3D printing, is a process used to manufacture 3D computer modelled objects, by adding one layer on top of another, as opposed to traditional formative or subtractive manufacturing methods. In this way it's possible to produce complex geometries with minimal material waste, which is ideal for prototypes or small production runs.

The limits of Additive Manufacturing are related to the material variety, the part size and the required post processing treatments that can lead to anisotropic mechanical properties. Another aspect of AM is the cost; for small scale production it's more convenient than formative and subtractive methods since different types of molds and tooling aren't needed but as the number of parts increases it becomes less convenient than the aforementioned methods, so the AM is used depending on the specific project requirements such as complexity, volume and cost efficiency.

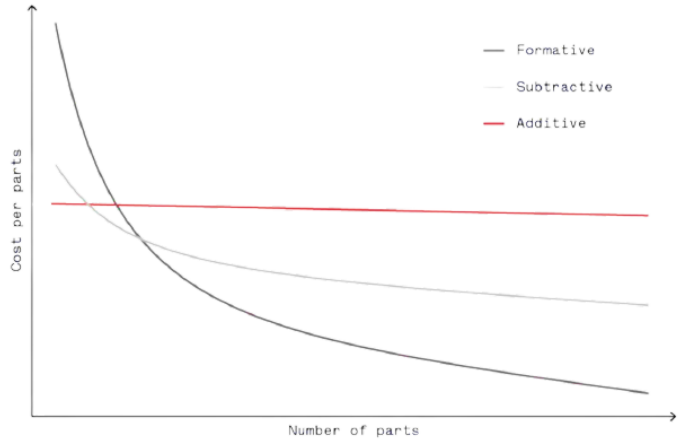

Figure 1.2: cost comparison between formative, subtractive and additive manufacturing method. [2]

There are different Additive Manufacturing techniques some examples are: Fused Deposition Modelling (FDM) where a thermoplastic filament in extruded through a heated nozzle, Stereolithography (SLA) which uses an UV laser to cure a photosensitive resin layer by layer, Digital Light Processing (DLP) that uses a digital light projector to cure photosensitive resins, Selective Laser Sintering (SLS) and Direct Metal Laser Sintering (DMLS) which are both powder bed fusion technologies based on laser sintering of powdered materials to bind them together into a solid structure; as for the SLS technique the materials processed are polymers and composites whereas for the DMLS process the materials treated are metals [2].

1.2.1 Direct ink writing

Additive manufacturing (AM) presents a revolutionary tool for scientists and engineers. Its design freedom unlocks advancements in diverse fields like biology, chemistry, and physics. Direct Ink Writing (DIW) emerges as a powerful AM technique due to its ability to handle a vast array of materials. This method works like a sophisticated extrusion system, constructing intricate 3D structures at the micro and meso scales. A computer-controlled stage precisely guides the deposition of a specialized ink, building the desired 3D object layer-by-layer.

DIW offers two primary methods: droplet and continuous extrusion. First introduced in 1997, DIW has seen explosive growth, attracting researchers for its simplicity, affordability, and ability to combine materials in a single step. Unlike other AM technologies, DIW isn't restricted by material type, as long as the material can be formulated into an ink with specific rheological properties.

One of DIW's greatest strengths lies in its ability to create multi-material structures in a single step. This streamlined process translates to significant advantages. Compared to traditional methods, DIW reduces overall manufacturing time, energy consumption, and waste generation. Notably, it achieves this efficiency without compromising the critical properties of the materials involved.

This rewrite emphasizes the efficiency gains and cost savings associated with DIW's multi-material printing capabilities.

Direct Ink Writing (DIW) is a layer-by-layer 3D printing technique that consist in extruding a viscoelastic ink through a fine nozzle by means of pressure.

The DIW process typically consists of three steps:

1. 3D Modeling: creating digital 3D models of the desired structures using Computer-Aided-Design (CAD) software;
2. Generating a 3D movement path for the nozzle using the appropriate software;
3. Ink Deposition: extruding the ink layer by layer to build the 3D structure.

Factors like nozzle size and printing speed significantly impact printing accuracy and resolution; smaller nozzles can enhance resolution, but require higher extrusion pressures and longer build times to prevent clogging whereas lower printing speeds lead to better shape accuracy and fidelity, but increase overall printing time.

Unlike other 3D printing techniques, DIW enables the extrusion of continuous filaments at room temperature. This is because printability relies on the ink's rheological properties rather than temperature. Therefore, optimizing the ink's rheological makeup is crucial and it can be achieved through various methods, such as chemical modification, the addition of rheological modifiers or fillers.

As the ink exits the nozzle, it undergoes bending and stretching before final deposition, the degree of stretching can be controlled by adjusting the ratio between extrusion rate and printhead movement speed.

After deposition, the ink solidifies through various mechanisms, including solvent evaporation, gelation, solvent-driven reactions, heat treatment, and photocuring.

DIW offers several benefits, such as minimal post-processing and reduced material waste, making it a more economical and sustainable manufacturing process. [3]

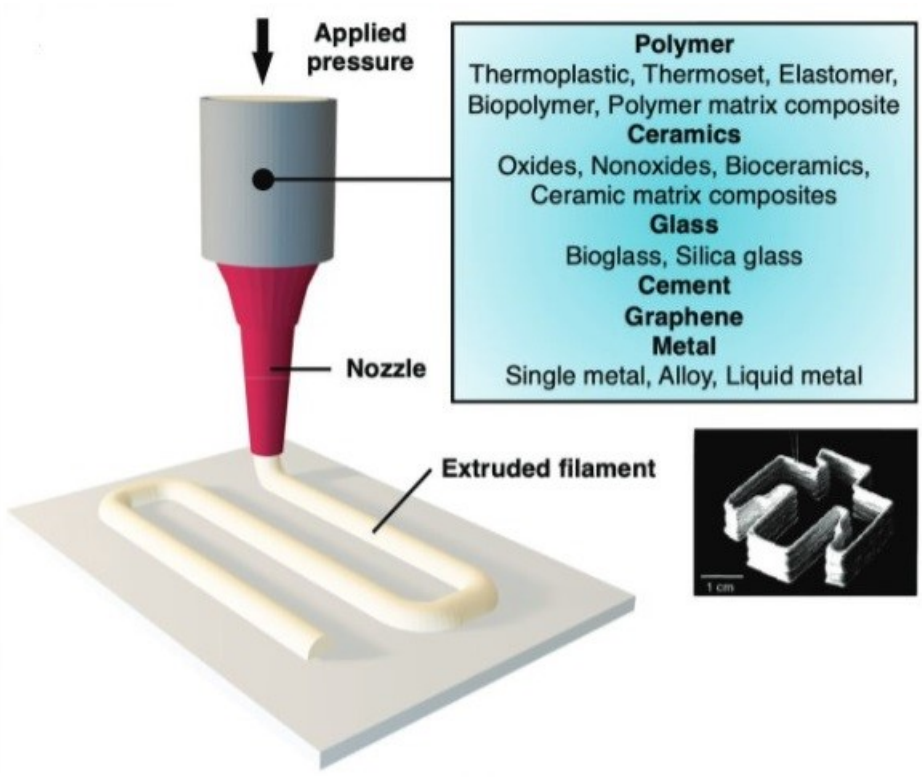

Figure 1.3: direct ink writing. [3]

Chapter 2 - Materials

2.1 Lithium Sulphate

Lithium Sulphate (Li_2SO_4) is an inorganic salt highly soluble in water, unlike most salts the solubility doesn't increase with temperature and it decreases when the temperature increases. Due to the hygroscopic character of the salt it is found most commonly in the monohydrate structure ($Li_2SO_4 \cdot H_2O$).

Lithium Sulphate possesses two crystallographic forms: a monoclinic one called β-Li_2SO_4 that converts into a cubic one at 572°C called α-Li_2SO_4, which is stable until the temperature of 860°C over which it melts.

If heated above 130°C it converts into a water free state, maintaining the monoclinic crystal structure.

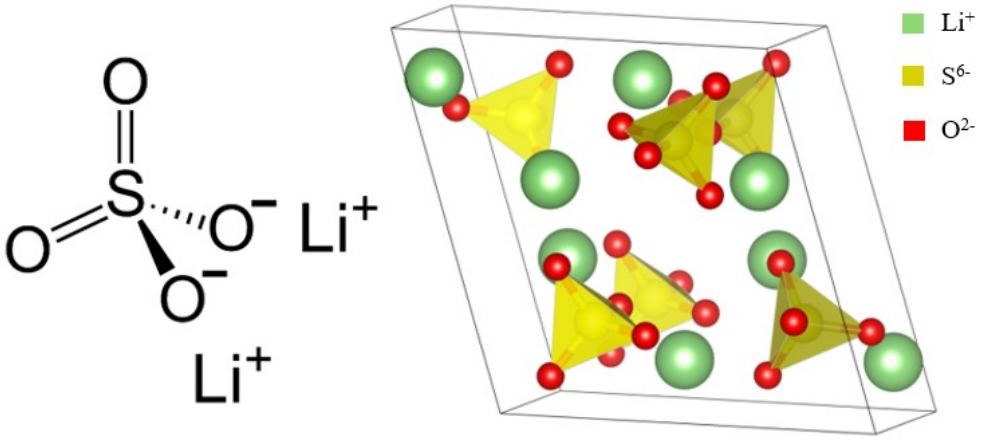

Figure 2.1: Li_2SO_4 structural formula on the left and unitary cell of β-Li_2SO_4 on the right. [https://en.wikipedia.org/wiki/Lithium_sulfate]

The salt is obtained by neutralization of lithium hydroxide with sulfuric acid followed by crystallization:

$$2LiOH + H_2SO_4 \rightarrow Li_2SO_4 + H_2O \quad (2.1)$$

Lithium Sulphate most common use is for the production of Lithium-ion batteries, more specifically the monohydrated form is used to make Lithium hydroxide (LiOH) which is used as cathode material in such batteries because it provides the Li^+ ions that are intercalated in electrically conductive materials for energy storage [1].

2.2 Sodium Sulphate

Sodium Sulphate (Na_2SO_4) in the anhydrous form, also called thenardite, is characterized by an orthorhombic structure and is highly hygroscopic, thus it absorbs water easily leading to the formation of a monoclinic decahydrate form ($Na_2SO_4 \cdot 10H_2O$) also called mirabilite.

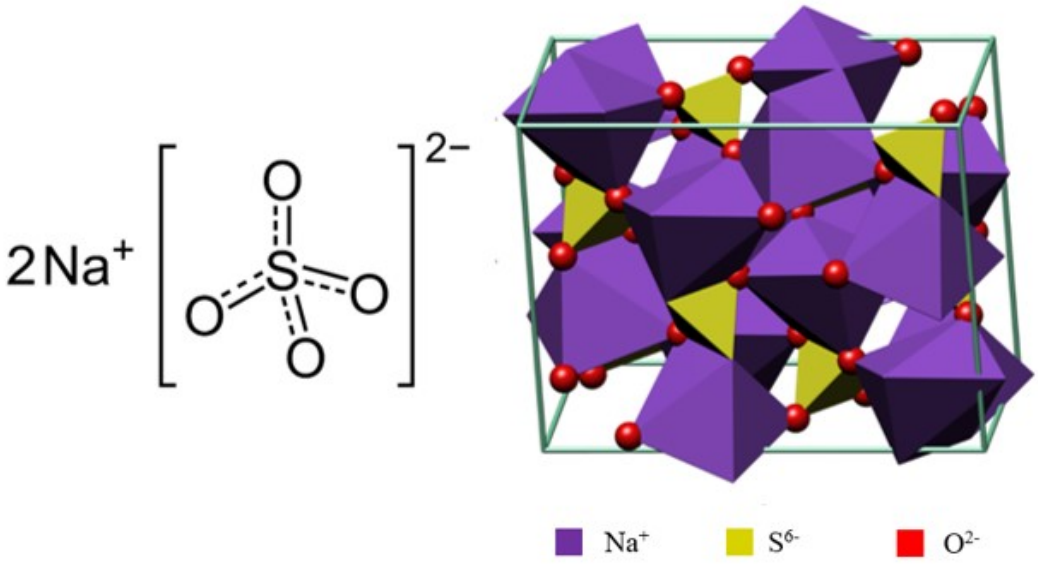

Figure 2.2: Na_2SO_4 structural formula on the left and anhydrous orthorhombic structure on the right. [https://en.wikipedia.org/wiki/Sodium_sulfate]

The anhydrite salt is obtained by the Mannheim process from the reaction between sodium chloride and sulfuric acid:

$$2NaCl + H_2SO_4 \rightarrow Na_2SO_4 + 2HCl \quad (2.2)$$

Another production method is the Hargreaves process where sulphur dioxide is used instead of sulfuric acid:

$$4NaCl + 2SO_2 + O_2 + 2H_2O \rightarrow 2Na_2SO_4 + 4HCl \quad (2.3)$$

In nature it is found on lakes and on dry river beds in the anhydrite form, while the decahydrate form can be found nearby saline springs and on dry saline lake beds.

For mass production it is usually purified from the decahydrate form by gentle warming so that the water slowly evaporates.

It is used in various sectors: it can be found in laundry detergents as a filler, in the glassmaking industry as a fining agent to remove air bubbles from molten glass and in space heating applications as an heat storage material; in this case the heat is stored in the solid to liquid phase change reaction which, in the decahydrate form, occurs at a temperature of 32°C [1].

2.3 Lithium and Sodium Sulphate System

The Li_2SO_4-Na_2SO_4 system was studied for thermal energy storage applications at high temperatures (450-550°C). The stoichiometric composition $LiNaSO_4$ is a superionic conductor that has a quasi-liquid cationic sub-lattice at 515°C, this means that the ions move as quickly as they would in a liquid, thus allowing heat to be transported into the lattice.

The study focused on two molar compositions: Li_2SO_4/Na_2SO_4 79/21 and Li_2SO_4/Na_2SO_4 50/50 corresponding to an eutectoid reaction and a solid-solid phase transition; the advantage of using this types of reactions is the possibility to achieve simple, compact and low costs thermal energy storage systems; this is due to the fact that for example in gas-solid or liquid-solid thermal energy storage systems two different phases must be stored separately in the first case and encapsulation is needed in the second case to prevent leakage. Moreover the phase transition is characterized by a fast kinetic due to the low energy barrier for the α-β phase conversion.

In the phase diagram reported below it's possible to observe the following eutectoid reaction at the composition Li_2SO_4/Na_2SO_4 79/21:

$$\beta\text{-}Li_2SO_4 + \beta\text{-}LiNaSO_4 \leftrightarrow \alpha\text{-}Li_2SO_4$$

The β-Li_2SO_4 phase is characterized, as already mentioned, by a monoclinic structure, the β-$LiNaSO_4$ phase is characterized by a trigonal structure and the α-Li_2SO_4 is characterized by a cubic structure [4].

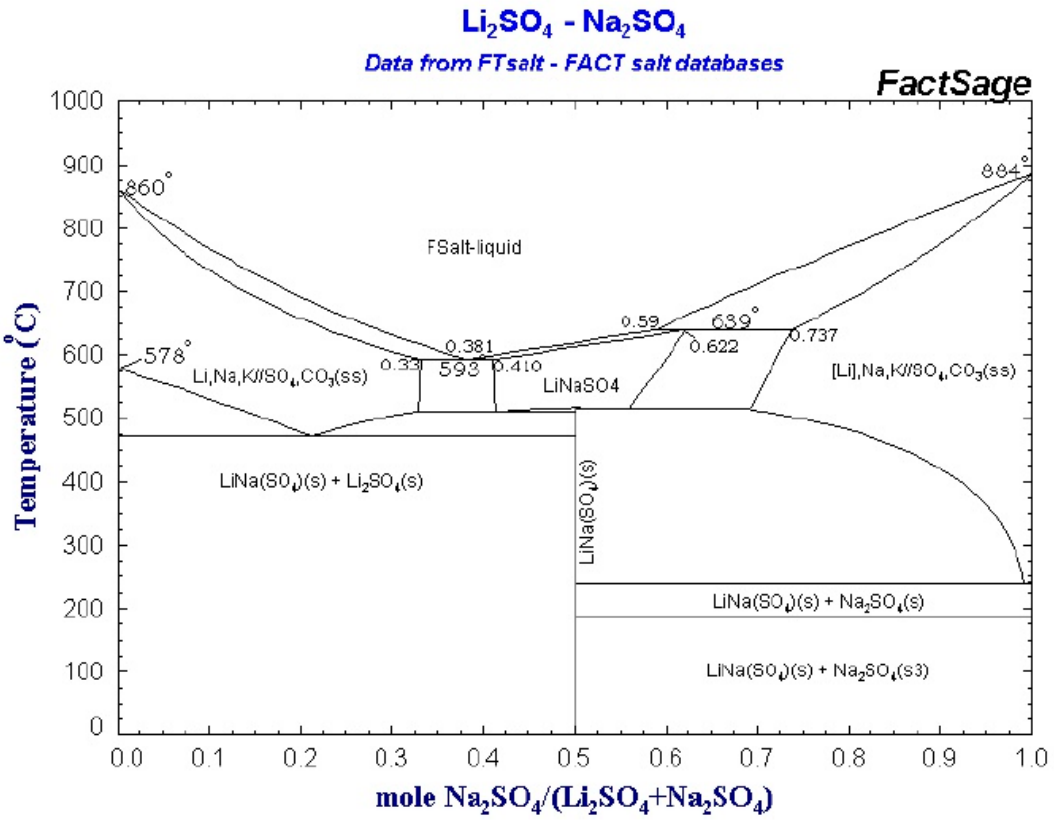

Figure 2.3: phase diagram of the Li_2SO_4-Na_2SO_4 system [5]

When the resulting compound $LiNaSO_4$ is heated the lattice parameters values, a and c, increase in a non linear way with increasing temperature and the increase in the c parameter is smaller than the increase in the a parameter [5][6].

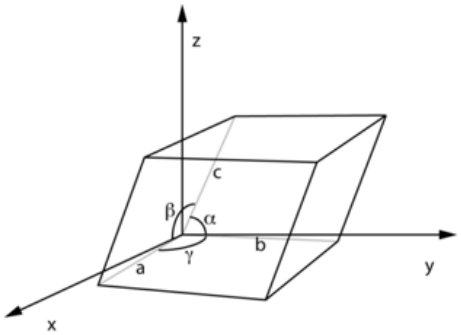

Temperature (° C)	Lattice parameter (nm)	
	a	*c*
30	0.763 23	0.986 18
100	0.764 61	0.987 44
155	0.765 74	0.988 56
200	0.767 16	0.989 65
262	0.769 02	0.990 54
318	0.770 41	0.990 80
375	0.773 38	0.991 58
424	0.774 97	0.991 15

Figure 2.4: on the left the lattice parameters "a,b,c" on a x,y,z oriented system and on the right the table reporting the variations of a and c with the temperature. [6]

It is possible to observe how the unit volume increases with increasing temperature.

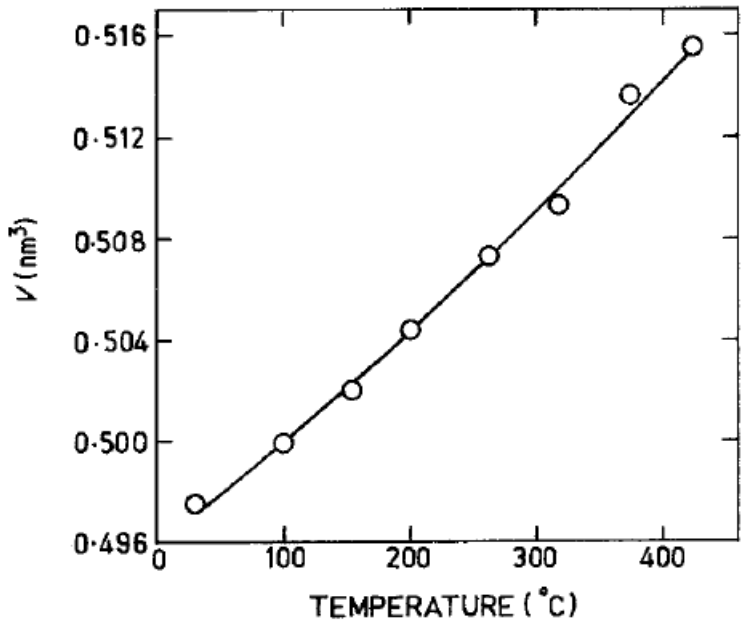

Figure 2.5: volume changes with temperature. [6]

2.4 Ethanol

Ethanol is an organic compound belonging to the alcohol family, its chemical formula is: CH_3CH_2OH. Ethanol is highly volatile and flamable. It's produced naturally from the fermentation of sugars by yeasts or synthetically by the hydration of ethylene.

The uses of ethanol are vary; it can be used as a fuel, as an antiseptic in the medical field, as a low-temperature liquid in laboratories to make cooling baths and as a solvent.

The chemical structure of Ethanol makes it suitable for the dissolution of polar, hydrophilic and non-polar hydrophobic compounds which is the reason why it is widely used as a solvent both in laboratories and in industrial processes.

The hydrogen bonding causes ethanol to be highly hygroscopic this means that it readily absorbs water from air.

Absolute ethanol was used as a solvent for this application; absolute ethanol is a low water content compound where the water content can range from 1% to ppm.

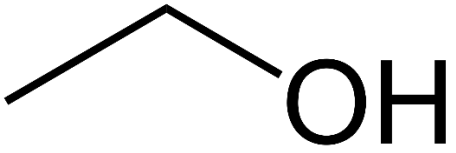

Figure 2.6: chemical structure of ethanol. [https://en.wikipedia.org/wiki/Ethanol]

2.5 Polyvinylpyrrolidone

Polyvinylpyrrolidone is a water soluble polymer made from the monomer of N-vynilpirrolidone.

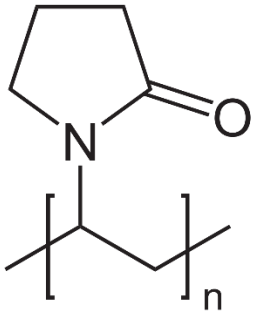

Figure 2.7: chemical structure of polyvinylpirrolidone. [https://en.wikipedia.org/wiki/Polyvinylpyrrolidone]

Its uses are multiple, it can be used together with iodine to make a complex called povidone-iodine which is an antiseptic widely used in the medical field, but it can be used in many other applications: as emulsifier, as an additive for batteries, ceramics, fiberglass, inks, etc., as a surfactant in nanoparticles synthesis, etc.

In this case it was used as a binder for the production, together with the salts, of a viscous ink.

Chapter 3 - Methods

3.1 Salts preparation

The two salts were prepared in order to make both the tablets and the ink, the following procedure was executed for each of the salt separately.

The Li_2SO_4 and the Na_2SO_4 salts were grinded with a ball milling machine and then sieved in order to obtain a very fine powder so as to increase the area of contact between the particles and to obtain finer grains which will lead to a more homogeneous ink for the printing phase.

The salts were milled using a milling machine; they were first put in an Agate jar then four spheres of the same material of the jar were added and the container was sealed (Figure 3.1).

They were then placed in the ball milling machine and milled at 350 rpm for 5 intervals of 10 minutes each with 4 minutes of pause between each interval in order to not overheat the machinery.

After the milling procedure the salts were sieved by using a 63 microns mesh.

Once this procedure was completed the salts were stored in hermetically sealed containers to prevent the hydration of the salts (due to the moisture present in the environment).

Figure 3.1: Agate jar with the powder and the Agate spheres inside on the left and the 63 micron sieve on the right.

3.2 Tablet preparation

The tablet were prepared according to the following molar ratios:

- 50/50 molar Li_2SO_4/Na_2SO_4;
- 79/21 molar Li_2SO_4/Na_2SO_4;
- 100/0 molar Li_2SO_4/Na_2SO_4.

The corresponding quantity in grams were the following:

Molar ratio	Li_2SO_4 [g]	Na_2SO_4 [g]	Total [g]
50/50	8	2.76	10.76
79/21	4	5.17	9.17
100/0	10	0	10

Table 3.1

The salts were weighted according to the quantity reported in the table, mixed and placed in three different containers, one for each molar ratio.

The powder mixtures were then pressed with a manual hydraulic press by using a metal stamp which had a hole of 5 mm diameter; a small metallic cylinder was first placed in the stamp and pushed at the bottom of it then the powder was added, and another one was placed on top of the powder. This ensemble was placed on top of a support and on the upper side of the stamp a piston with the same diameter of the small metallic cylinders was placed in correspondence of the hole and the upper screw of the press shown in Figure 3.2 was spinned until everything was secure and still.

By using the handle a pressure of 5 ton was applied, leaving the salt mixture at that pressure for about 1 minute, then the force was released and the formed tabled was carefully removed from the stamp. The removal of the tablet from the stamp was critical because it didn't come off by hand but it needed to be removed using the pressure exerted by the piston so to make the tablet exit from the other side of the stamp which had instead of the previously used support an hollow metal cylinder under it.

10 tablets for each molar composition were obtained and thermally treated. It was observed that the tablets were quite frail and could easily break apart, especially the ones made only of Li_2SO_4.

Figure 3.2: manual hydraulic press on the left and the stamp with the small metallic cylinders inside on the right.

3.3 Ink preparation

In order to prepare the ink the following substance were used:

- Li_2SO_4;
- Na_2SO_4;
- Absolute Ethanol;
- Polyvinylpyrrolidone (PVP).

The instrument used were:

- THINKY ARE-250 orbital mixer.

Two composition were printed:

- 50/50 molar Na_2SO_4-Li_2SO_4;
- 100/0 molar Na_2SO_4-Li_2SO_4;

In order to make a printable ink it was necessary to mix the salts with Ethanol and PVP; in this way a paste is obtained, the quantity used are reported in Table 3.2 and 3.3.
In order to prepare the ink a preblend of Ethanol and PVP was made, with a ratio of 0.69g of PVP every 2.31g of Ethanol.

Reagent	Mass [g]	% wt
Na_2SO_4	10.00	78
EtOH	2.16	17
PVP	0.65	5

Table 3.2

Reagent	Mass [g]	% wt
Na_2SO_4	4.64	34
Li_2SO_4	6	44
EtOH	2.31	17
PVP	0.65	5

Table 3.3

The salts were weighted in a plastic container, the preblend was then added to achieve the right viscosity. It's important to add the liquid preblend as the last step in order to prevent the evaporation of the Ethanol.

The container was sealed and placed in an orbital mixer where it was mixed at 2000rpm for 2 minutes.

Figure 3.3: THINKY ARE-250 orbital mixer.

For both of the composition after the mixing step the container was opened and exposed to air for about 1 minute in order to achieve the right viscosity for printing. After leaving it in air for the required time the mixture presented a dryer layer on the surface due to the

evaporation of the Ethanol that occurs first on the layer in closer contact with the air; so to homogenize the mixture it was mixed again at 2000rpm for 30 seconds.
After the final mixing step it was left to cool in the fridge, inside the closed container for about 2 minutes.

3.4 Direct ink writing

The instrument used for printing were:

- 30 cc syringe;
- piston and cap for the 30cc syringe;
- 0.58 mm tip;
- VIEWEG DC 300 pressure regulator;
- Delta 2040 Turbo 2 printer.

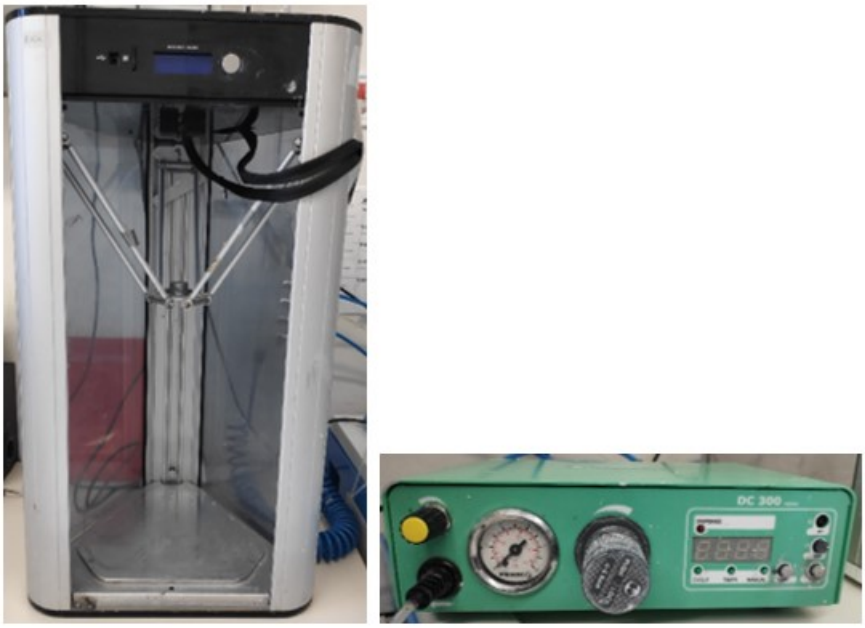

Figure 3.4: Delta 2040 Turbo 2 printer on the left and VIEWEG DC 300 pressure regulator on the right.

The previously cooled ink was quickly poured, by using a metal spatula, into the syringe which was closed on the bottom side with a cap.
The piston was inserted into the syringe and pushed towards the bottom so to put it directly in contact with the ink, the cap was removed, and the 0.58 mm tip was applied.

Finally the syringe was connected to the pressure regulator and the pressure was raised until the liquid started to come out of the tip of the syringe in order to find a value that during printing would be kept constant (Figure 3.5)

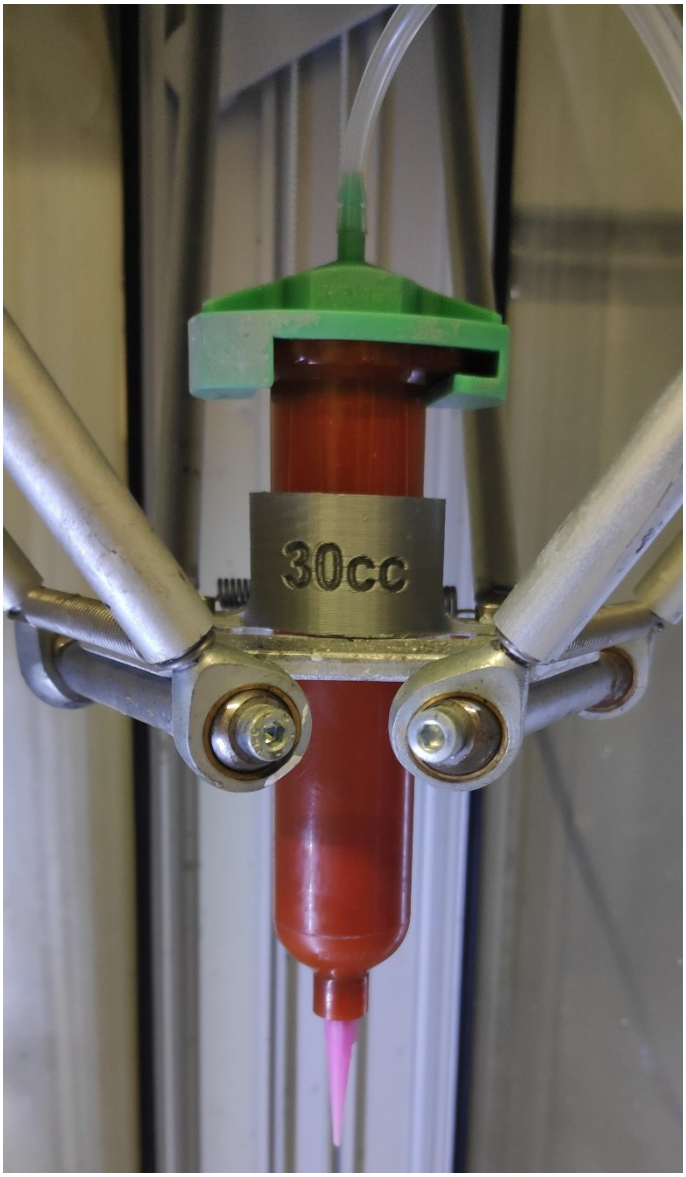

Figure 3.5: syringe with the piston inside, the 0,58 mm tip, all connected with the pressure regulator.

The pressure at which the ink was printed was slightly above 0 bar, the exact value is unknown due to the sensitivity of the tool but it could be estimated to be around 0.1 bar. A parafilm foil was placed on the base of the printer and the ink was printed continuously on the foil at a constant pressure, during the printing a jet of compressed air needs to be directed on the printed filament to accelerate the evaporation of ethanol thus drying the

printed section; if the air is not applied then the structure will slightly collapse on the centre due to the too high liquid component.

After printing the components were left to dry on an open plastic container for a day.

The geometry printed were mainly three, each with different porosity percentages and straight lines and one geometry presented a wavy sinusoidal line shape:

- 50% porosity, straight lines:
  - composition 100/0;
- 60% porosity, straight lines:
  - composition 100/0;
- Wavy sinusoidal:
  - composition 100/0;
  - composition 50/50.

3.5 Thermal treatments

The thermal treatments were performed on both the tablets and the structured components.

As for the tablets they were thermally treated by placing in an oven three tablets with the three different molar composition for each of the following ramps:

- Ramp 1: 300°C for 30 minutes, 400°C for 30 minutes, 525°C for 2 hours, at a 2°C/min temperature increase rate;
- Ramp 2: 200°C for 6 hours at a 1°C/min temperature increase rate;
- Ramp 3: 300°C for 6 hours at a 1°C/min temperature increase rate;
- Ramp 4: 400°C for 6 hours at a 1°C/min temperature increase rate;
- Ramp 5: 500°C for 6 hours at a 2°C/min temperature increase rate;
- Ramp 6: 600°C for 6 hours at a 2°C/min temperature increase rate;
- Ramp 7: 700°C for 6 hours at a 2°C/min temperature increase rate.

Regarding the structured components for each geometry 13 components were produced and thermally treated with Ramp 1. For the 50% porosity ones another 13 were made in order to compare the mechanical properties of thermally non-treated components.

3.6 XRD analysis

The XRD analysis is used to characterize and quantify the mineral constituents of a material and the position of the atoms in the lattice.

When X-rays impinge on solid materials, they are scattered by the electrons revolving around atom's nucleus. These scattered waves interfere with each other and the nature of the interference can be constructive or destructive (Figure 3.17).

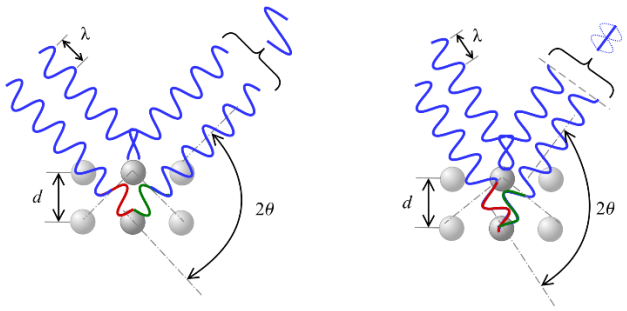

Figure 3.17: constructive interference on the left and destructive interference on the right.

If the interference is constructive, meaning that the rays superimpose with each other, then diffraction takes place because the wavelength of the X-rays is similar to the interatomic spacings in the crystal. These constructive interactions produce the X-ray diffraction pattern used for crystal structure determination.

W. L. Bragg found that diffracted X-rays act as if reflected from a family of planes (called Bragg's planes) which are the rows of atoms that make up the crystal structure.

The reflection occurs when the following equation is satisfied:

$$n(\lambda) = 2d \sin\theta \tag{3.1}$$

It's possible to observe that constructive interference occurs when the length $2dsen\theta$ is equal to an integer multiple of the wavelength of the radiation ($n(\lambda)$) whereas destructive interference occurs for n equal to a fractional number [7].

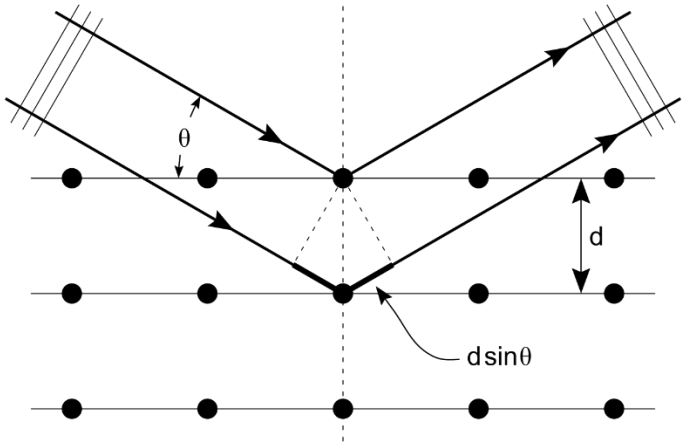

Figure 3.18: two beams that have the same wavelength and phase approach a crystalline solid and are scattered off by two different atoms. The lower beam traverses an extra length of 2dsinθ.

3.7 Mechanical properties

The fracture behaviour of brittle materials, specifically ceramics, typically initiates from the presence of distributed defects within the material. The strength of a specimen is influenced by the dimensions of its primary defects, which can differ from one specimen to another. Consequently, the mechanical strength of brittle materials is best characterized by a statistical probability function. The Weibull distribution function serves as the foundation for contemporary mechanical design methodologies for ceramic components. The fundamental premise is that failure occurs when the weakest volume element of the specimen fails. Experimental evidence indicates that the likelihood of fracture escalates with both the applied load and the size of the specimen. The Weibull distribution is a statistical model frequently employed to represent reliability data and failure durations. It was first proposed by Wallodi Weibull, a Swedish engineer and mathematician, during the 1950s. A key characteristic of ceramic materials is their inherent brittleness and the variability in defect distribution, which greatly affects the unpredictability of failure and compromises the reliability of experimental fracture data. This underlines the prevalence of the Weibull distribution as the preferred method for describing the mechanical strength of ceramics. When the rupture outcomes from a sufficient number of samples are represented in a histogram, this data can be analytically described using a function known as the Weibull distribution density [8]:

$$f\left(\frac{\sigma}{\sigma_0}\right) = \frac{m}{\sigma_0} \cdot \left(\frac{\sigma}{\sigma_0}\right)^{m-1} \cdot exp\left[\left(\frac{\sigma}{\sigma_0}\right)^{m}\right]$$

(3.1)

where m is the Weibull module, σ is the fracture stress, and σ0 is a normalisation parameter.

As the m-value increases, the distribution becomes narrower, which is expressed in a higher accuracy of the fracture data. The survival probability for a given σ value can instead be expressed in two ways:

$$S = exp\left[-\left(\frac{\sigma}{\sigma_0}\right)^{m}\right]$$

(3.2)

$$ln\ ln\frac{1}{S} = m\ ln\frac{\sigma}{\sigma_0} = m\ln\sigma - m\ln\sigma_0$$

(3.3)

In a graphical representation of ln ln(1/S) against ln σ, it is possible to derive the parameters m and σ_0 from experimental data, subsequently allowing for the calculation of S for each σ value. To ascertain the values of m and σ_0, it is essential to construct the Weibull plot for each batch. This involves arranging the fracture stress values of the N samples in ascending order. For each specimen, the associated survival probability S_j can be determined using the following approximate relationship:

$$S_j = \frac{j - a}{N + b}$$

(3.4)

where a and b are two parameters, comprised between 0-1.0 and 0-0.5 respectively, whose value depends on N.

3.8 Energy Dispersive X-ray Spectroscopy (EDS)

Energy Dispersive X-ray Spectroscopy (EDS) is a powerful technique integrated into SEM (section 4.4) to analyse the elemental composition of a sample. A focused electron beam excites atoms, causing them to emit characteristic X-rays. These X-rays are detected and analysed to identify and quantify the elements present in the sample.

X-rays emitted from the sample are captured by an Energy Dispersive X-ray (EDS) detector. This detector, typically a solid-state semiconductor crystal like silicon, converts each incoming X-ray photon into a small electrical pulse. The energy of the pulse directly correlates with the energy of the X-ray photon.

The collected X-rays are then sorted and analysed by an energy-dispersive spectrometer. This device separates the X-rays based on their energy levels, directing them towards the detector. The detector measures the energy of each X-ray, generating a spectrum that reveals the elemental composition of the sample.

An EDS spectrum is often visualized as a graph. The x-axis represents the energy of the X-rays, while the y-axis indicates the number of X-rays detected at each energy level. Peaks on this graph correspond to specific elements present in the sample, and the height of each peak signifies the relative abundance of that element.

Beyond imaging, SEM finds applications in a wide range of fields, including materials science, quality control, failure analysis, and biological research. It's a versatile tool that provides valuable insights into the surface characteristics, structure, and composition of materials. In this case it was used to analyse the distribution of atoms in the thermally treated and non thermally treated samples.

3.9 Scanning Electron Microscopy (SEM)

A beam of high-energy electrons, typically ranging from 0.1 to 30 keV, is focused onto a sample surface in a vacuum chamber. This primary electron beam interacts with the atoms on the surface, triggering a series of emissions, including secondary electrons, backscattered electrons, and X-rays.

Secondary electrons, the most commonly used signal in Scanning Electron Microscopy (SEM), originate from inelastic collisions near the sample's surface. These low-energy electrons provide detailed information about surface topography and texture.

Backscattered electrons, on the other hand, are higher-energy electrons that penetrate deeper into the sample before being scattered back. They offer insights into the sample's composition, as their intensity varies with atomic number.

The emitted electrons are captured by detectors, converted into electrical signals, amplified, and processed to generate an image. By systematically scanning the electron

beam across the sample, a high-resolution image is formed, revealing intricate details at magnifications from 10x to over 4000x.

3.10 Thermal Performances: DSC analysis

Differential scanning calorimetry (DSC) is a thermal analysis technique that measures alterations in a material's heat capacity as its temperature changes. This method is employed to examine thermal properties, assess material purity, and identify stability and phase transitions. In a DSC analysis, the sample and a reference material undergo a controlled temperature program, either increasing or decreasing gradually. As the temperature fluctuates, the heat flow necessary to maintain both the sample and reference at identical temperatures is monitored. Any disparity in heat flow between the sample and reference is recorded as a signal, indicating thermal events occurring within the sample material.

Chapter 4 – Results

4.1 Thermal treatments

The results after the thermal treatment of the tablets can be observed in the following pictures.

Ramp 1:

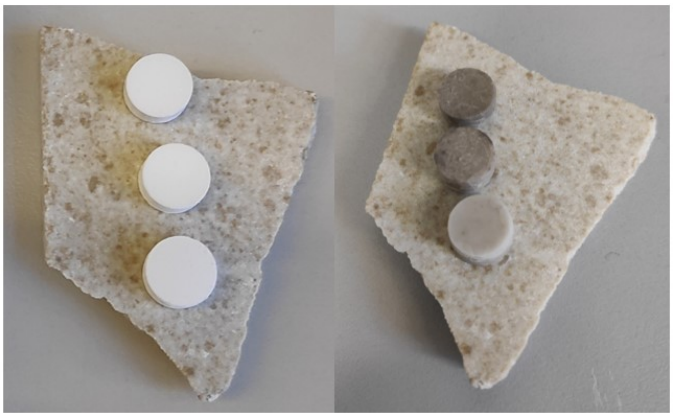

Figure 4.1: tablets before (left) and after (right) thermal treatment, in order from top to bottom 50/50 molar, 79/21 molar and 100/0 molar.

Ramp 2:

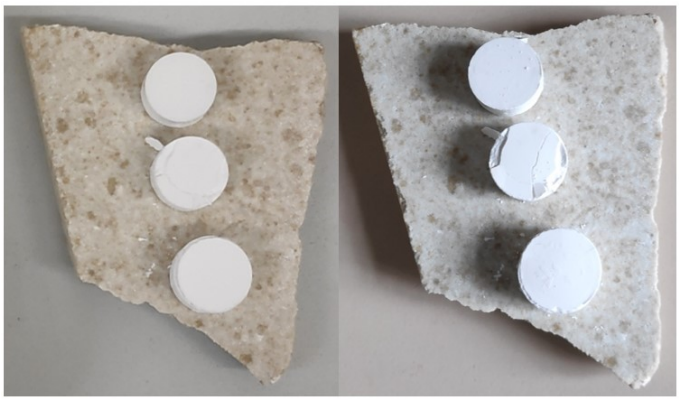

Figure 4.2: tablets before (left) and after (right) thermal treatment, in order from top to bottom 50/50 molar, 79/21 molar and 100/0 molar.

Ramp 3:

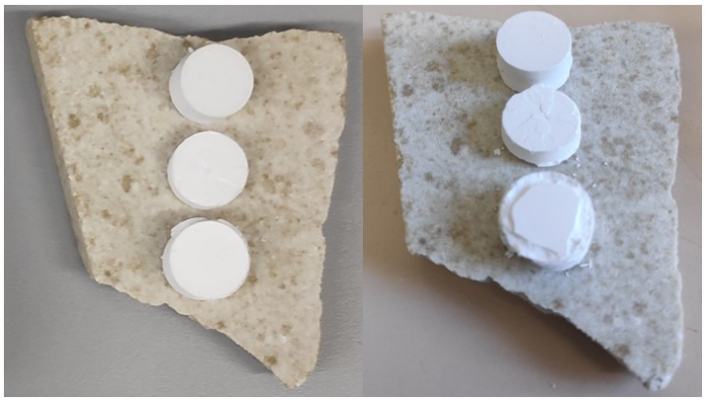

Figure 4.3: tablets before (left) and after (right) thermal treatment, in order from top to bottom 50/50 molar, 79/21 molar and 100/0 molar.

Ramp 4:

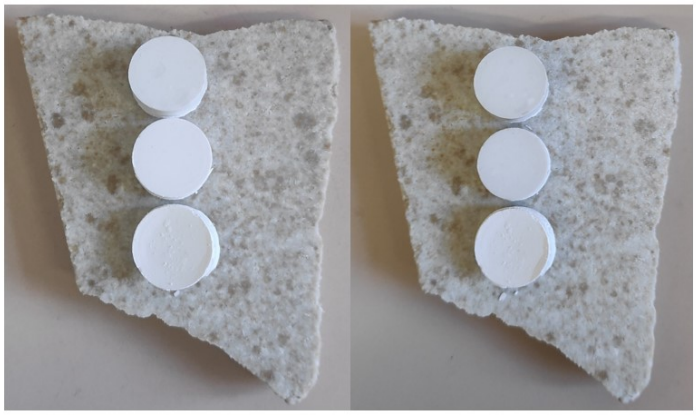

Figure 4.4: tablets before (left) and after (right) thermal treatment, in order from top to bottom 50/50 molar, 79/21 molar and 100/0 molar.

Ramp 5:

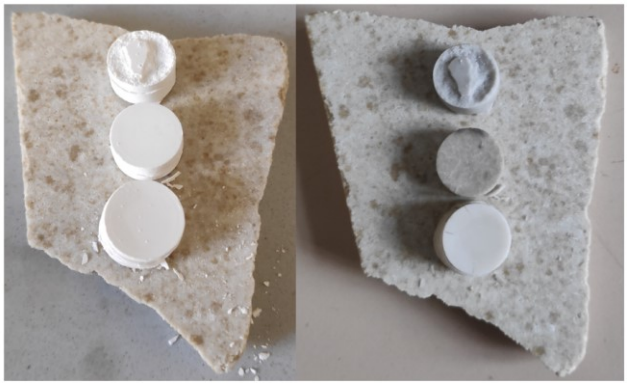

Figure 4.5: tablets before (left) and after (right) thermal treatment, in order from top to bottom 50/50 molar, 79/21 molar and 100/0 molar.

Ramp 6:

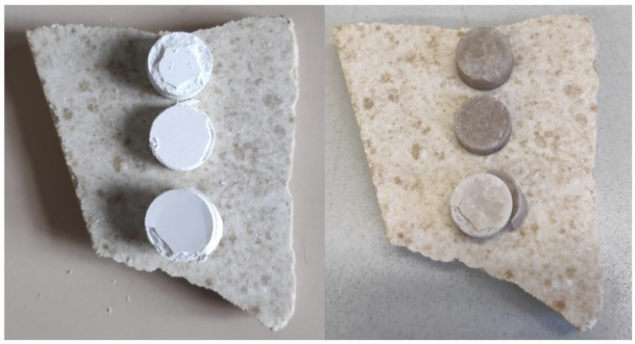

Figure 4.6: tablets before (left) and after (right) thermal treatment, in order from top to bottom 50/50 molar, 79/21 molar and 100/0 molar.

Ramp 7:

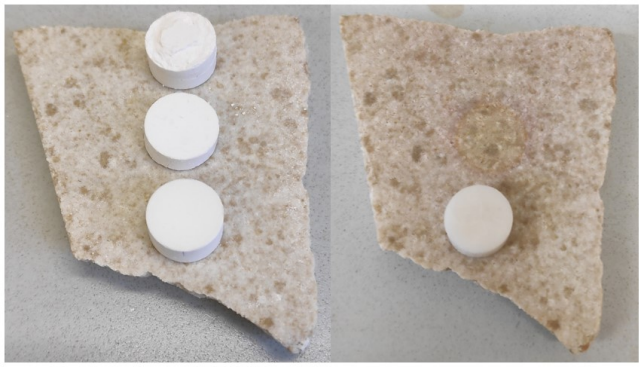

Figure 4.7: tablets before (left) and after (right) thermal treatment, in order from top to bottom 50/50 molar, 79/21 molar and 100/0 molar.

It's possible to observe that by going over 500°C the tablets containing Na_2SO_4 becomes darker (tending to a grey colour) and the higher the content of the Na_2SO_4 the darker the tablet becomes while the ones containing only Li_2SO_4 remains unvaried in colour. The darkness slightly increases at higher temperatures as it can be seen in Figure 4.1, 4.5 and 4.6.

At 700°C the tablets containing Li_2SO_4 and Na_2SO_4 melts in agreement with the phase diagram (Figure 4.8) and the only surviving tablet is the one made of only Li_2SO_4 [9].

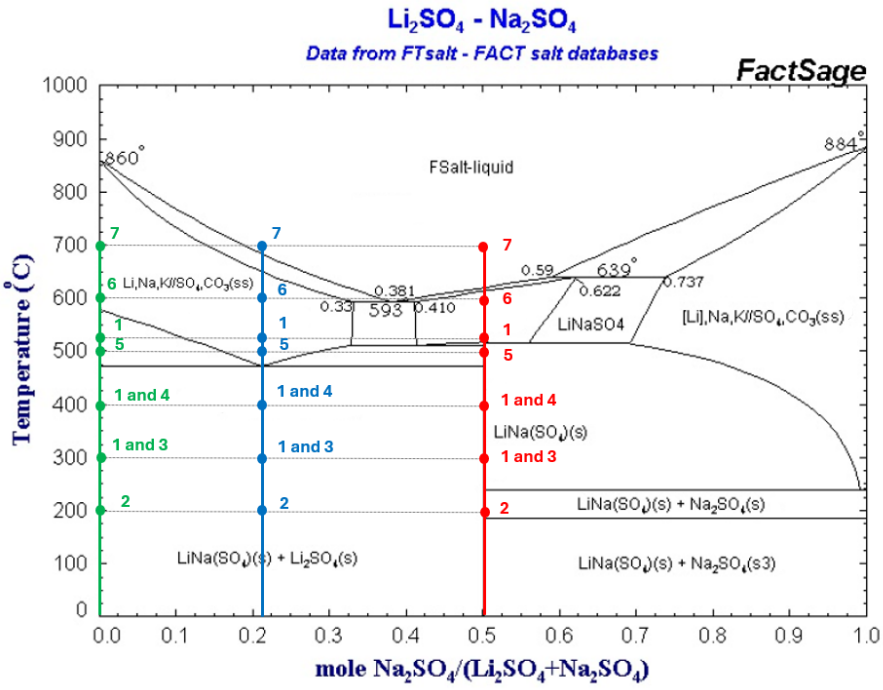

• 100/0 molar Li_2SO_4/Na_2SO_4; • 79/21 molar Li_2SO_4/Na_2SO_4; • 50/50 molar Li_2SO_4/Na_2SO_4.

Figure 4.8: the number of the thermal ramps reported on the phase diagram for each molar composition. [5]

Regarding the structured components the thermal treatment performed was the same as Ramp 1 of the tablets. It's possible to observe that even for the 100% Na_2SO_4 ones there is a change in colour when thermally treated.

Figure 4.9: 50% porosity components before (top) and after (bottom) heating treatment.

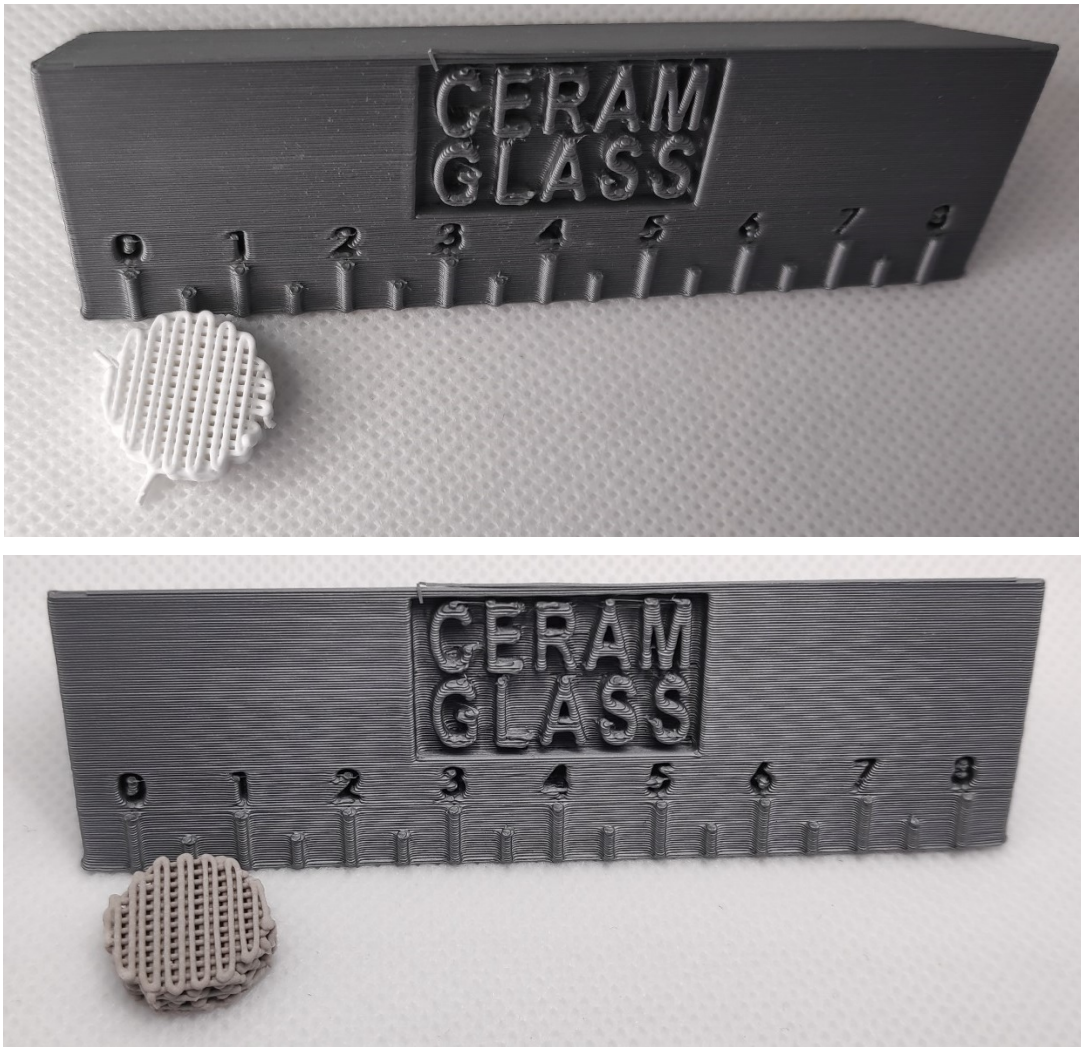

Figure 4.10: 60% porosity components before (top) and after (bottom) heating treatment.

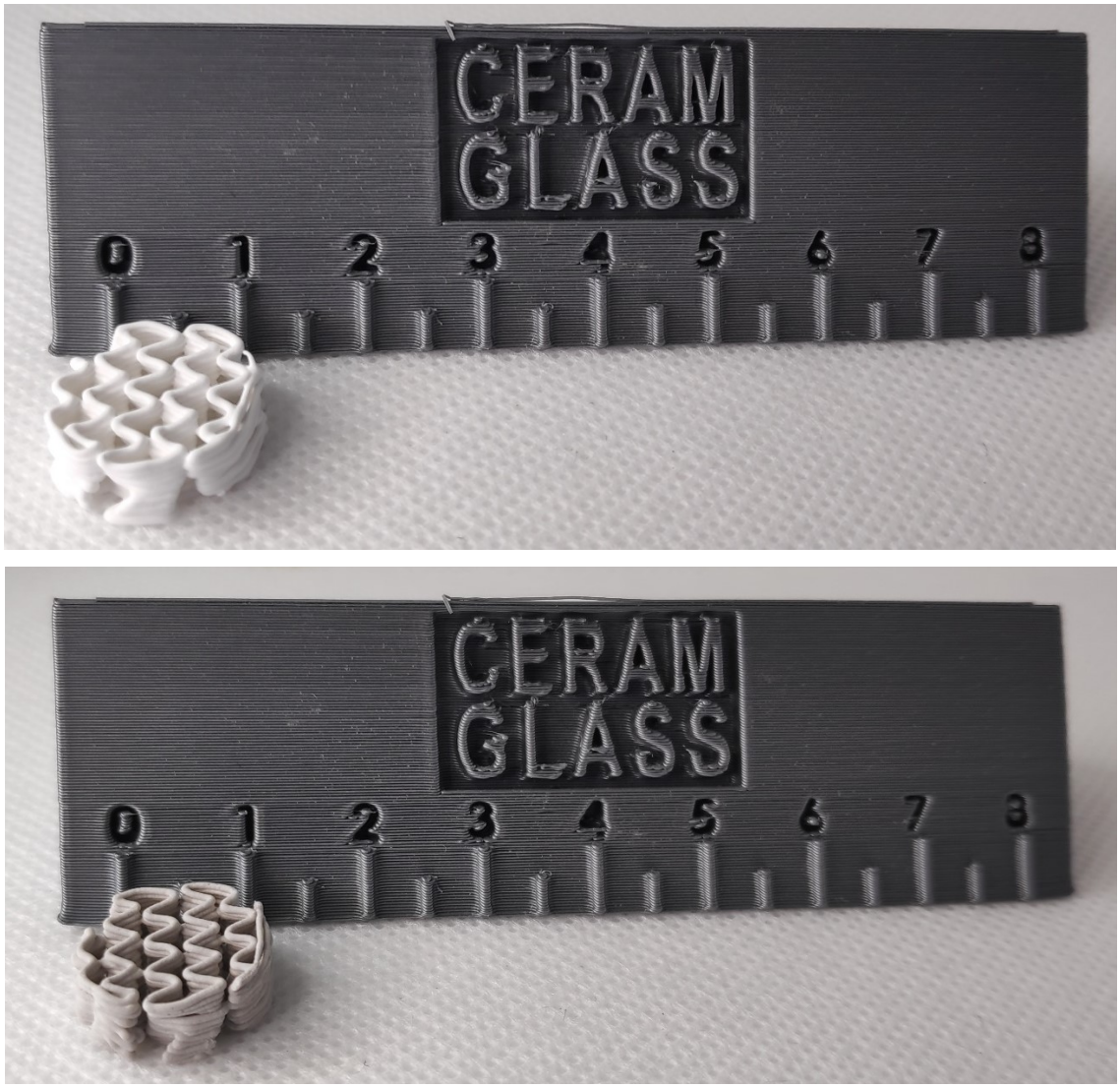

Figure 4.11: wavy sinusoidal components before (top) and after (bottom) heating treatment.

As mentioned before it's possible to observe that by going over 500°C the tablets acquire a darker colour, tending to grey, and the more Na_2SO_4 is present the darker the tablets or the structured components become. This could be attributed to the fact that at high concentrations, Na_2SO_4 acts as a liquid phase that penetrates between the particles, dissolving the sinter bonds and promoting particle rearrangement. This accelerated liquid-phase sintering process may lead to larger, irregular particles and a worsening of the 79/21 and 50/50 sample's colour due to excessive crystal growth like in the case of addition of Na_2SO_4 on TiO_2 (Figure 4.12) [10].

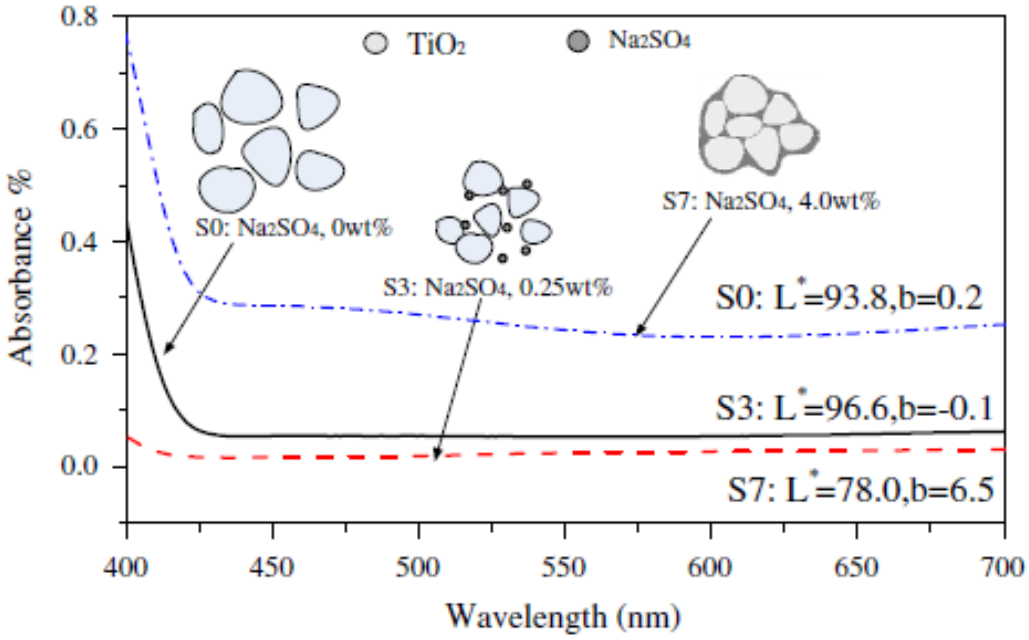

Figure 4.12: absorbance of TiO_2 and Na_2SO_4 mixture. L indicates lightness and b indicates blue-yellow colour component; for higher Na_2SO_4 content the absorbance of the samples increases. [10]*

4.2 XRD analysis

The XRD analysis was carried out to assess the accuracy of the phase diagram and to better understand the reason of the colour change in the tablets containing both salts. It's possible to state that the colour change is due to the reaction between sodium sulphate and lithium sulphate since it occurs only in the tablets containing the combination of the two.

From the XRD it can be observed that for the darker tablets the only compound found was $LiNaSO_4$ so it can be said that over 500°C the only compound that is responsible for the colour change is Na_2SO_4, although to assess the reason of the colour change a study on the light absorbance, crystal growth and crystal morphology of the $LiNaSO_4$ system should be carried out.

As for the XRD analysis of the samples patterns were recorded in a 2θ angular range of 10–120° with a step size of 0.02° and a step time of 1.5 s, the results for each thermal ramp are shown in the graphs below.

It's possible to observe in Figure 4.13 how in the composition 79/21 molar small traces of Li_2SO_4 are found in agreement with the phase diagram.

For Figure 4.14 the presence of hydrates found in the composition 79/21 and 50/50 are due to the long times required for the XRD analysis which can lead to the absorption of water molecules from the atmosphere; the hydration can also occur during the storage time of the tablets, the same consideration can be made for all of the other graphs where hydrated compounds are present.
For Figures 4.15, 4.16, 4.17, 4.18 and 4.19 all the phases found were in agreement with the phase diagram.

Ramp 1: 300°C for 30 minutes, 400°C for 30 minutes, 525°C for 2 hours, at a 2°C/min temperature increase rate.

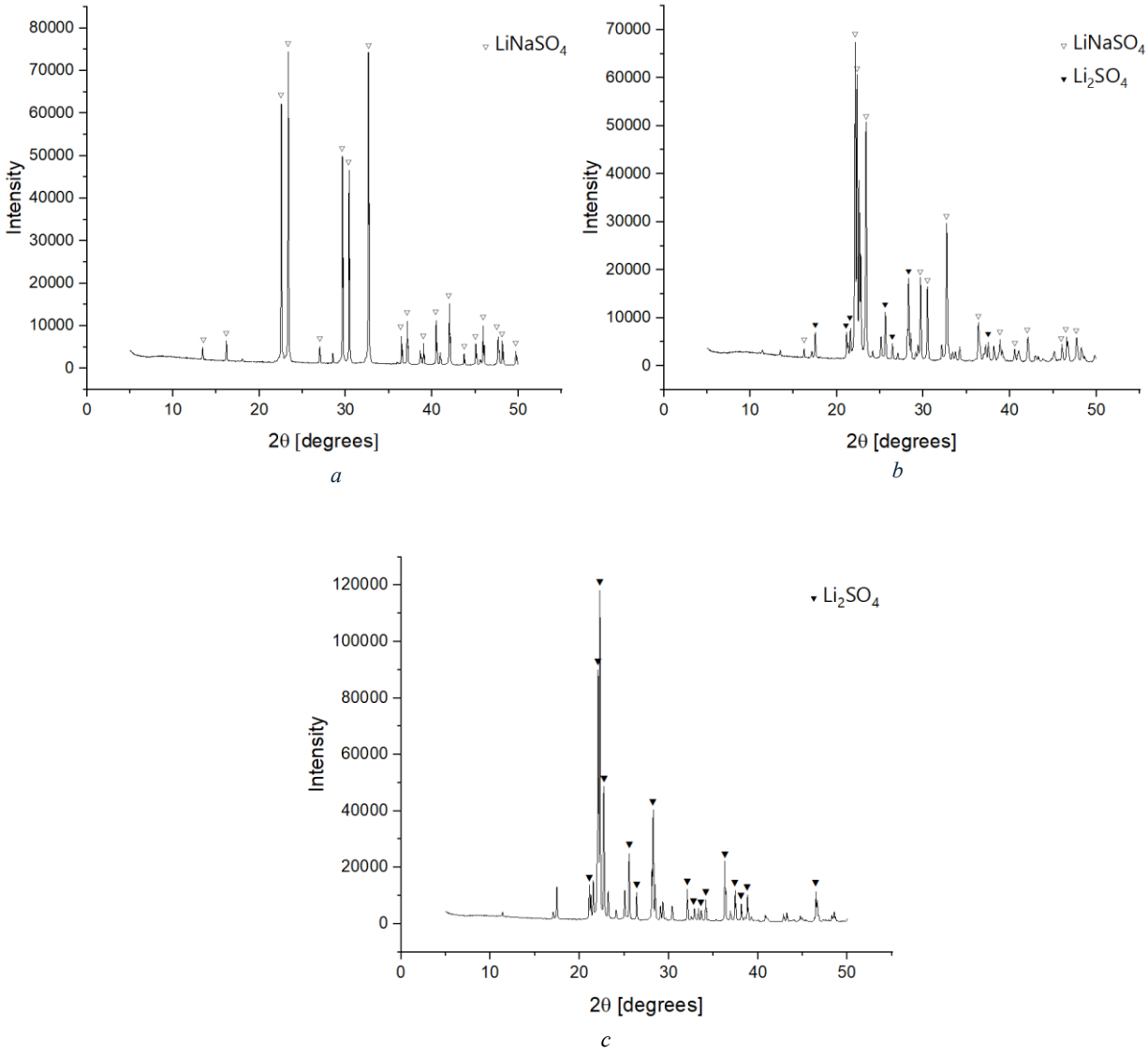

Figure 4.13: XRD patterns for Ramp 1: a 50/50; b 79/21; c 100/0.

Ramp 2: 200°C for 6 hours at a 1°C/min temperature increase rate.

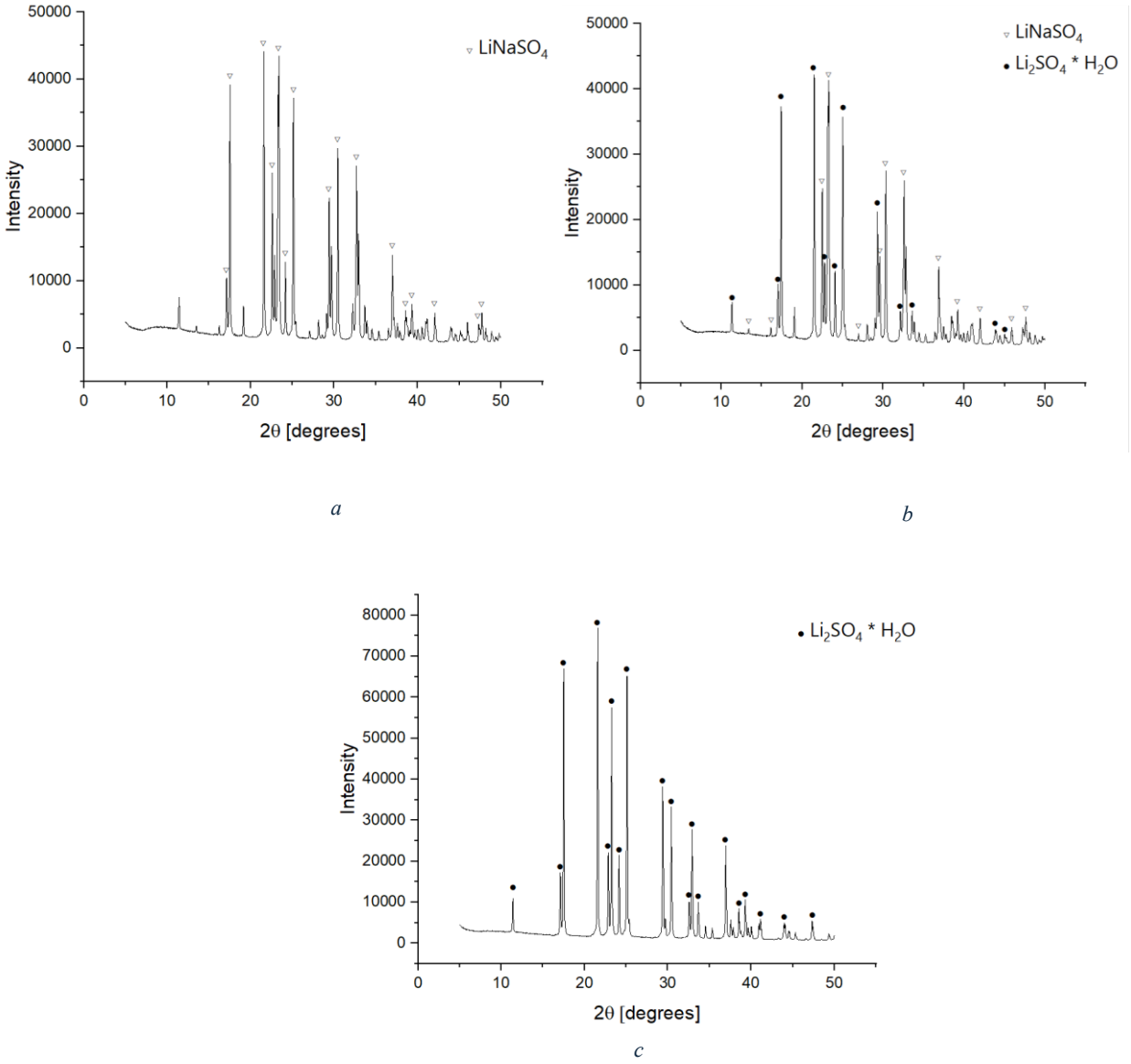

Figure 4.14: XRD patterns for Ramp 2: a 50/50; b 79/21; c 100/0.

Ramp 3: 300°C for 6 hours at a 1°C/min temperature increase rate.

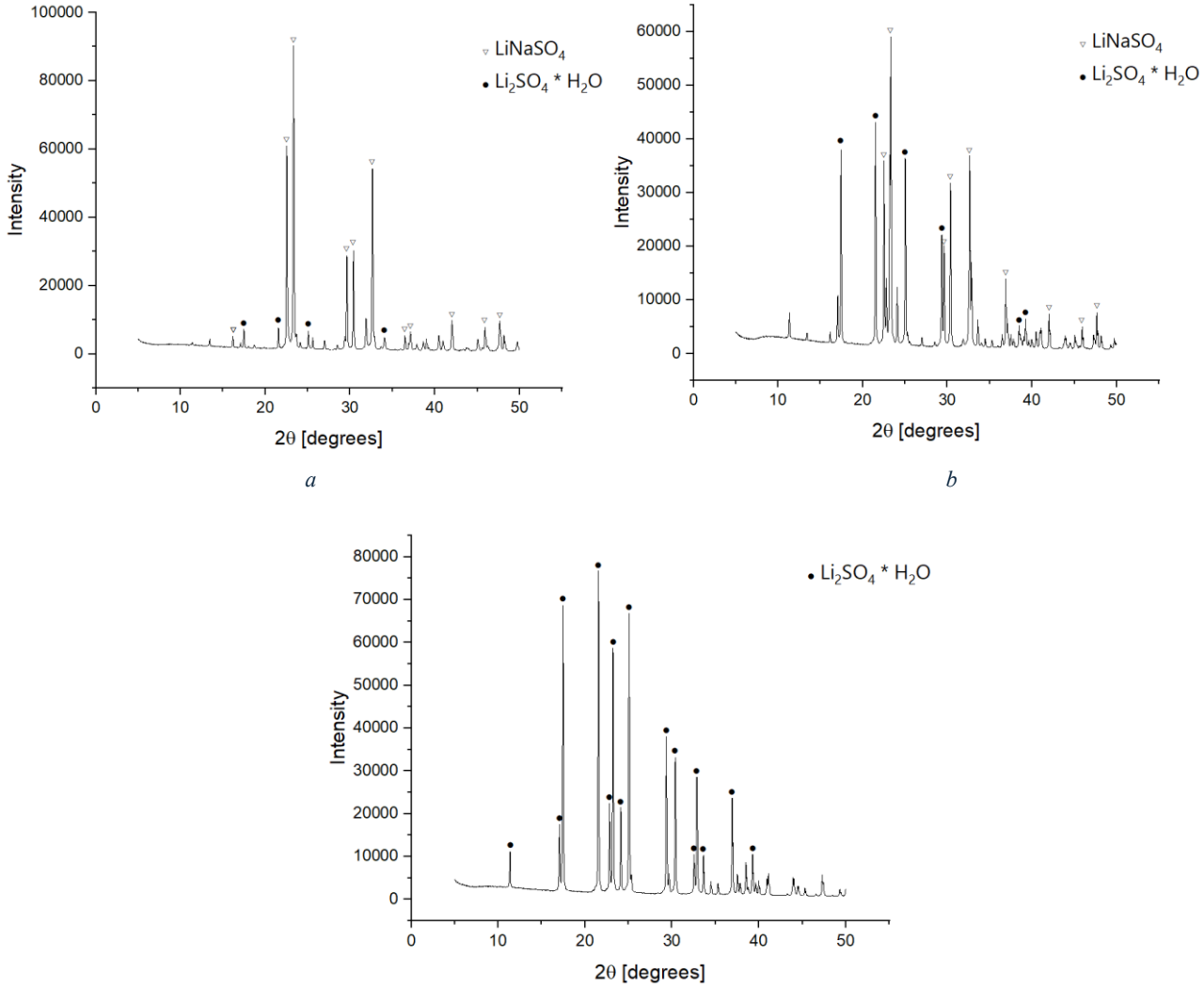

Figure 4.15: XRD patterns for Ramp 3: a 50/50; b 79/21; c 100/0.

Ramp 4: 400°C for 6 hours at a 1°C/min temperature increase rate.

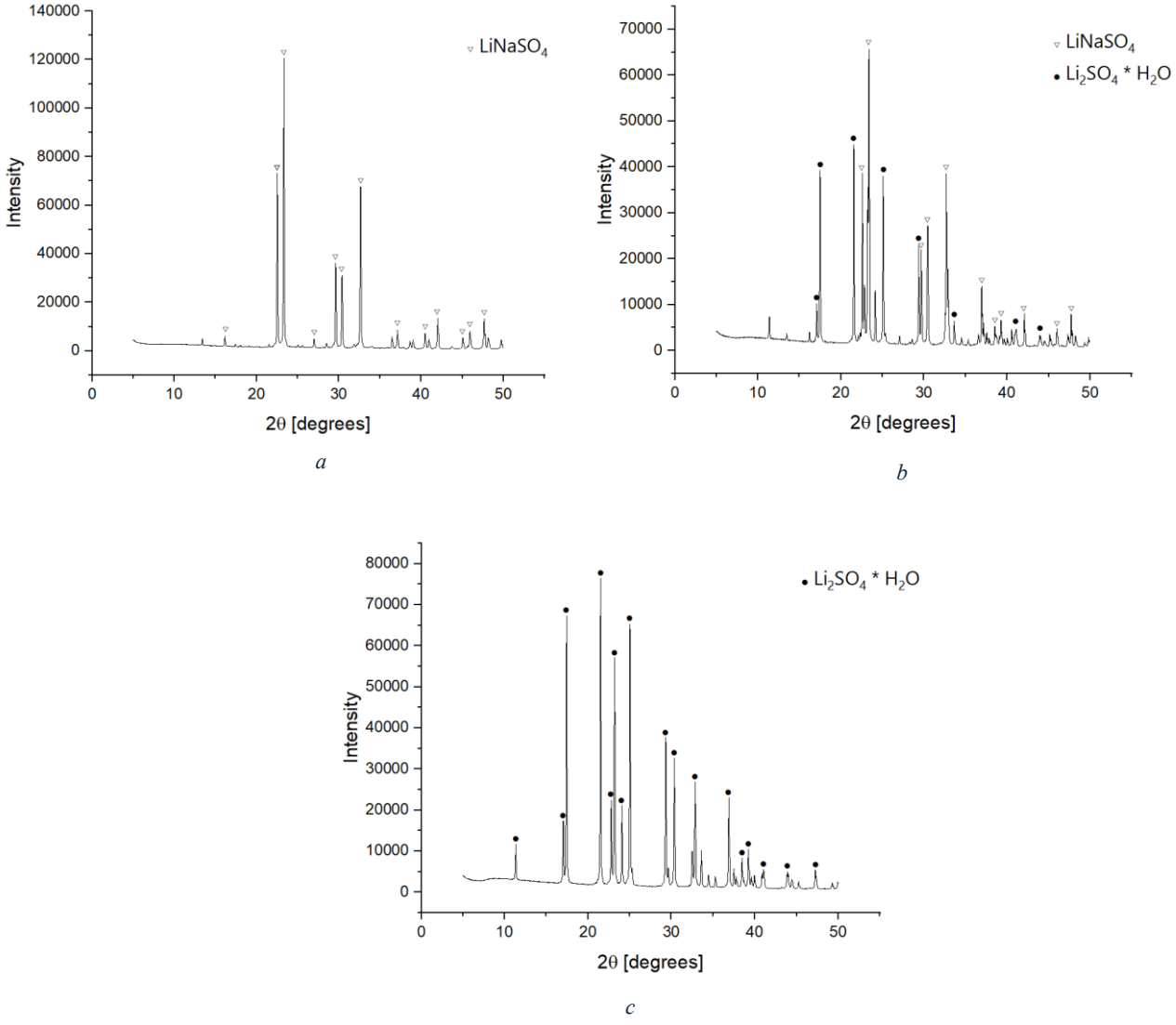

Figure 4.16: XRD patterns for Ramp 4: a 50/50; b 79/21; c 100/0.

Ramp 5: 500°C for 6 hours at a 2°C/min temperature increase rate.

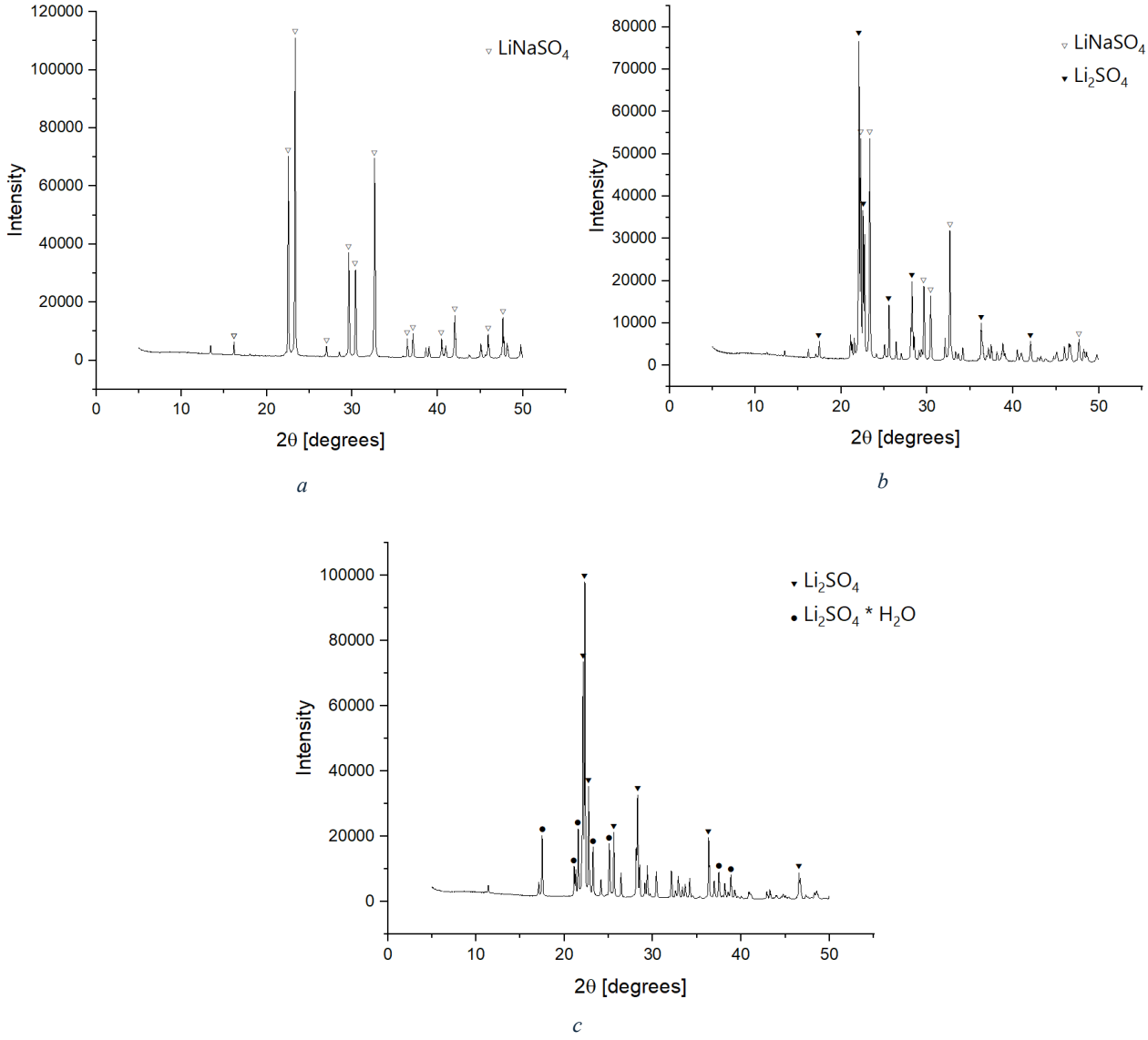

Figure 4.17: XRD patterns for Ramp 5: a 50/50; b 79/21; c 100/0.

Ramp 6: 600°C for 6 hours at a 2°C/min temperature increase rate.

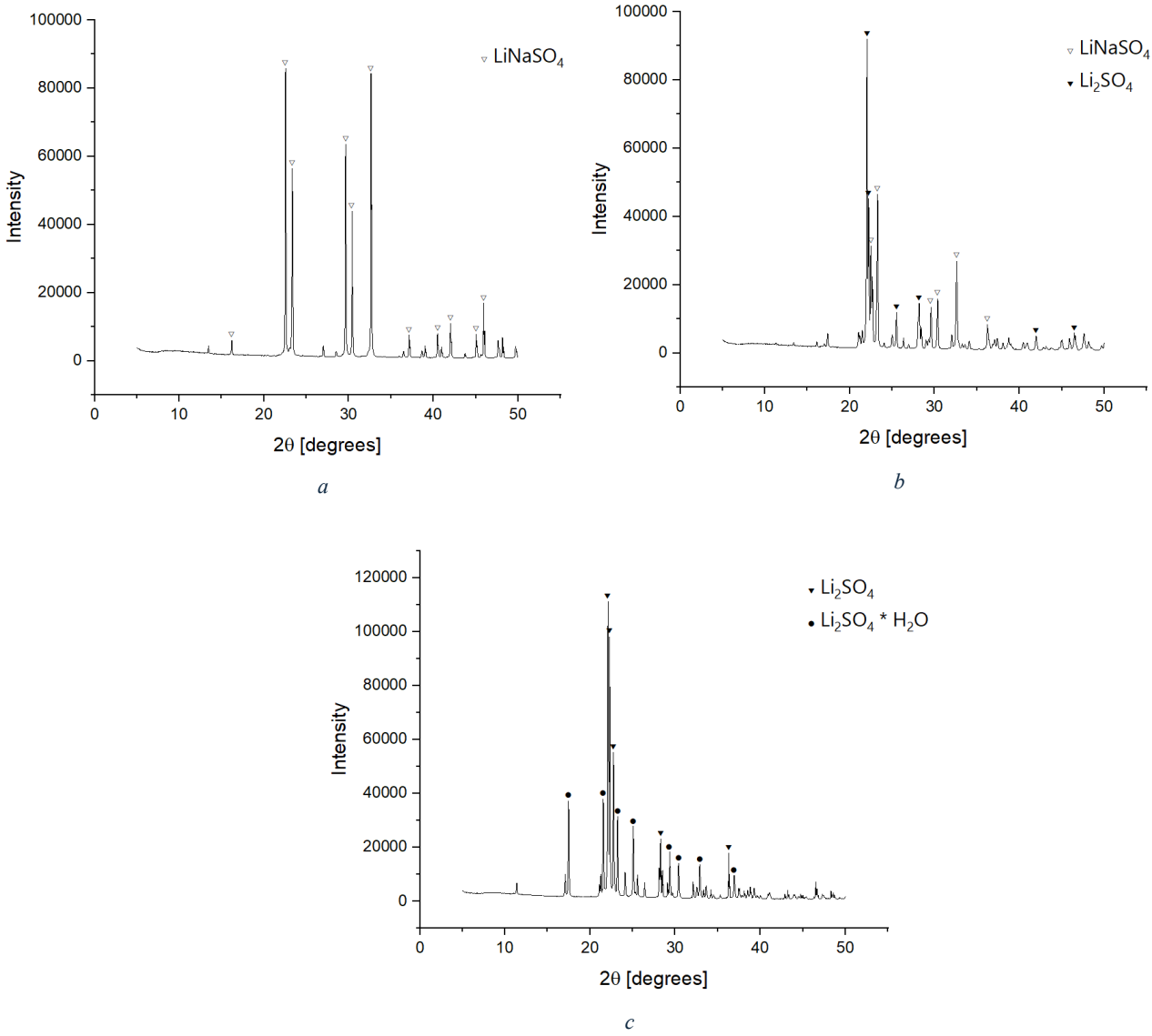

Figure 4.18: XRD patterns for Ramp 6: a 50/50; b 79/21; c 100/0.

Ramp 7: 700°C for 6 hours at a 2°C/min temperature increase rate.

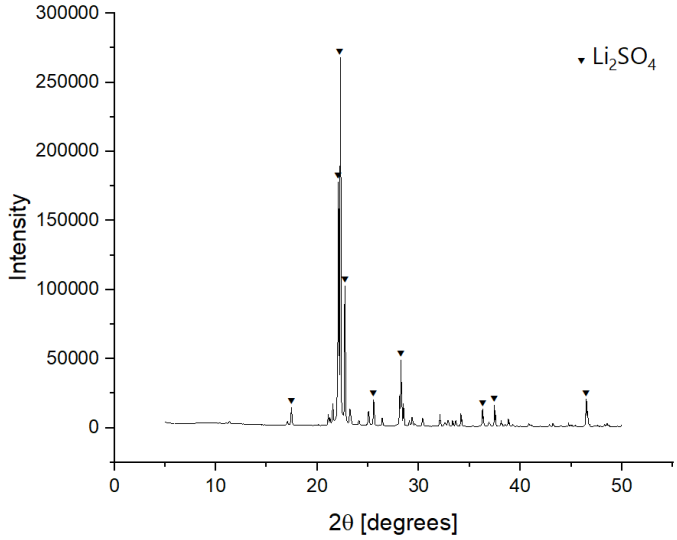

Figure 4.19: XRD patterns for Ramp 7 for 100/0.

From the XRD analysis performed on the Na_2SO_4 structured components before and after the heating treatment no significant changes were detected, small differences in the peaks are present but, looking at figure 4.20, the composition remains the same.

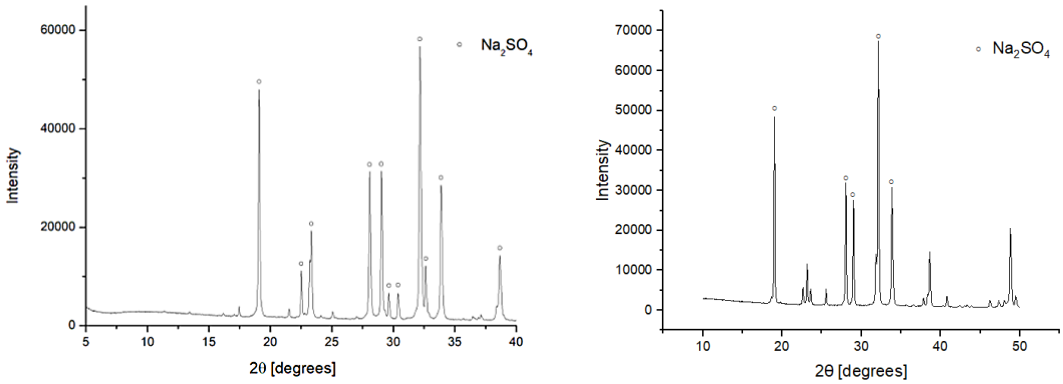

a *b*

Figure 4.20: XRD pattern for 100 mol Na_2SO_4: a non heat treated sample, b heat treated sample.

4.3 Mechanical properties

The tables below show data on dimensions, stress at break and survival probability for each of the tested components. The mechanical performances of both heat treated and non heat treated geometries were studied. For each geometry 13 specimen were tested.
To summarise the tested specimens were the following:

- 50% porosity, straight lines, heat treated;
- 60% porosity, straight lines, heat treated;
- Wavy sinusoidal, heat treated;
- 50% porosity, straight lines not heat treated.

Compression test results in terms of Weibull Parameters, the number of specimens tested N and the parameters a and b are reported in table 4.1.

Specimen	N	m	σ_0 [MPa]	a	b
Wavy sin ht	13	2.56	2.71	0.50	0.00
50% ht	13	2.81	5.58	0.50	0.00
60% ht	13	2.89	3.27	0.50	0.00
50% no ht	13	2.95	63.99	0.50	0.00

Table 4.1

The values obtained for the stress at break for each specimen are very different, this is due to the fact that the geometry and in particular the porosity affects the mechanical properties of the samples. Other factors to take in account of for the high variability of these values are presence of cracks that may have generated during the heating treatment or eventual air bubbles that formed during the printing phase.
The Weibull modulus is in the range of the one possessed by traditional ceramics (brick, pottery, chalk), much lower than the one of engineered ceramics which is comprised between 5 and 10. [12]
By looking at tables 4.2, 4.3, 4.4 and 4.5 it can also be noted that the survival probability is the highest for the sample that failed for a lower value of stress; as the stress at break increases the survival probability decreases and so the failure probability increases.
The following observation can be made considering the data reported in the aforementioned tables: for the specimens that were subjected to an heating treatment the values of stress at break are significantly lower and the one that presents higher

mechanical properties is the one that has 50% porosity and straight lines. This is understandable because if the porosity is higher and the filament diameter and disposition is the same, then the filament lines are lower in amount, so the resistance to the compressive stress applied is lower. On the contrary if the porosity is lower (50%) then there's a more resistant structure that can support the compressive stress.

For the specimen with a wavy profile it's possible to note that having the filament not intertwined caused lower values of fracture stress.

Although the amount of porosity decreases the mechanical properties it is still needed in order to accommodate the volumetric changes that occurs in the material during the heating treatment.

Another important factor that must be taken in account of is the heating treatment; the non heat treated sample had the highest value of stress at break, this can be explained by the fact that the heating treatment eliminates completely PVP, Ethanol and eventual water thus producing a brittle component where the movement of the atoms subjected to a stress is hindered by the predominant ionic bonding.

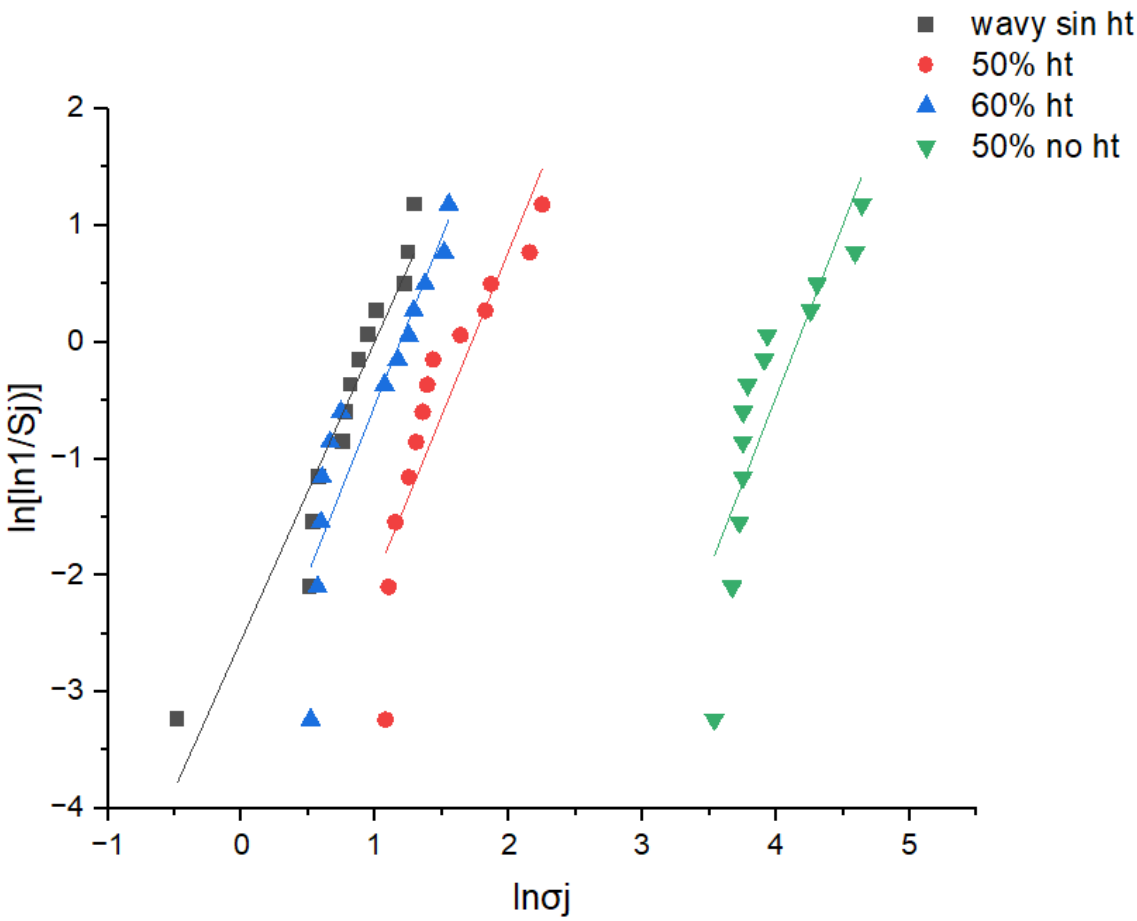

Figure 4.21: Weibull linear fit.

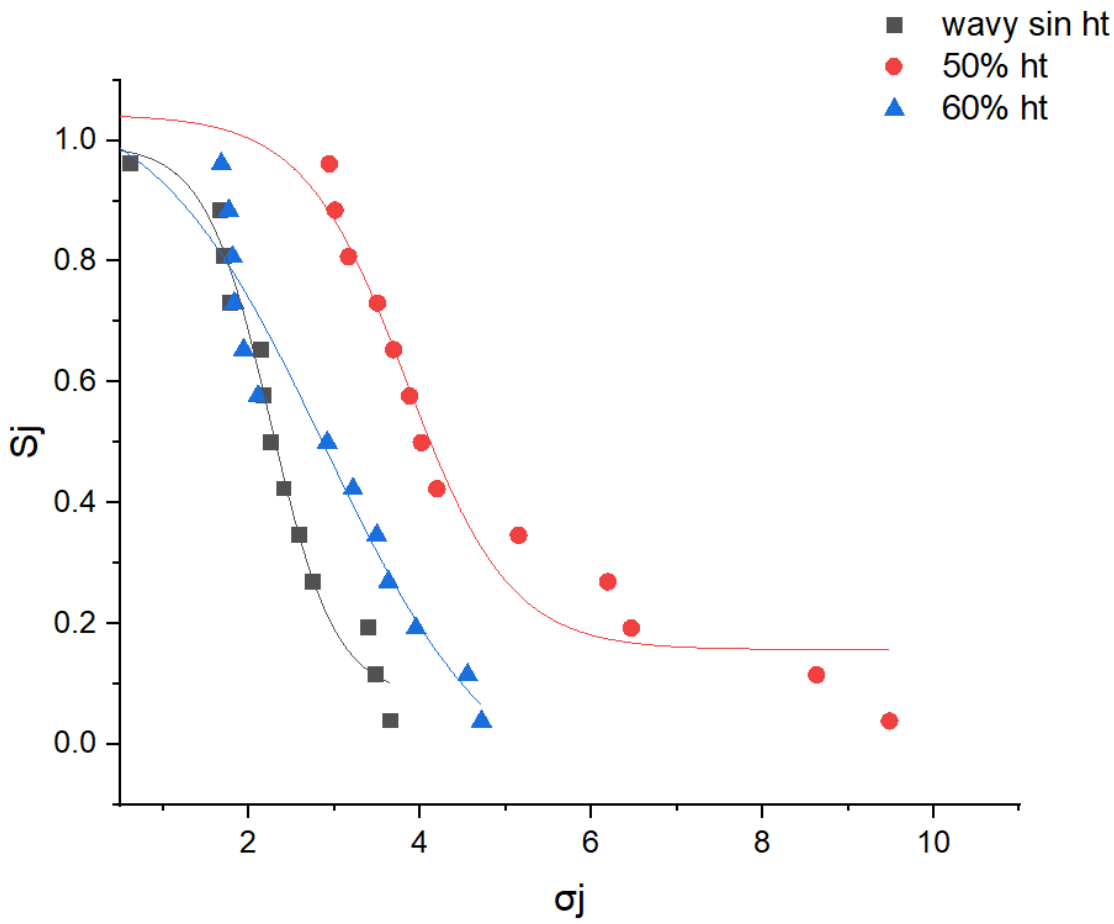

Figure 4.22: Weibull exponential fit only for the heat treated samples.

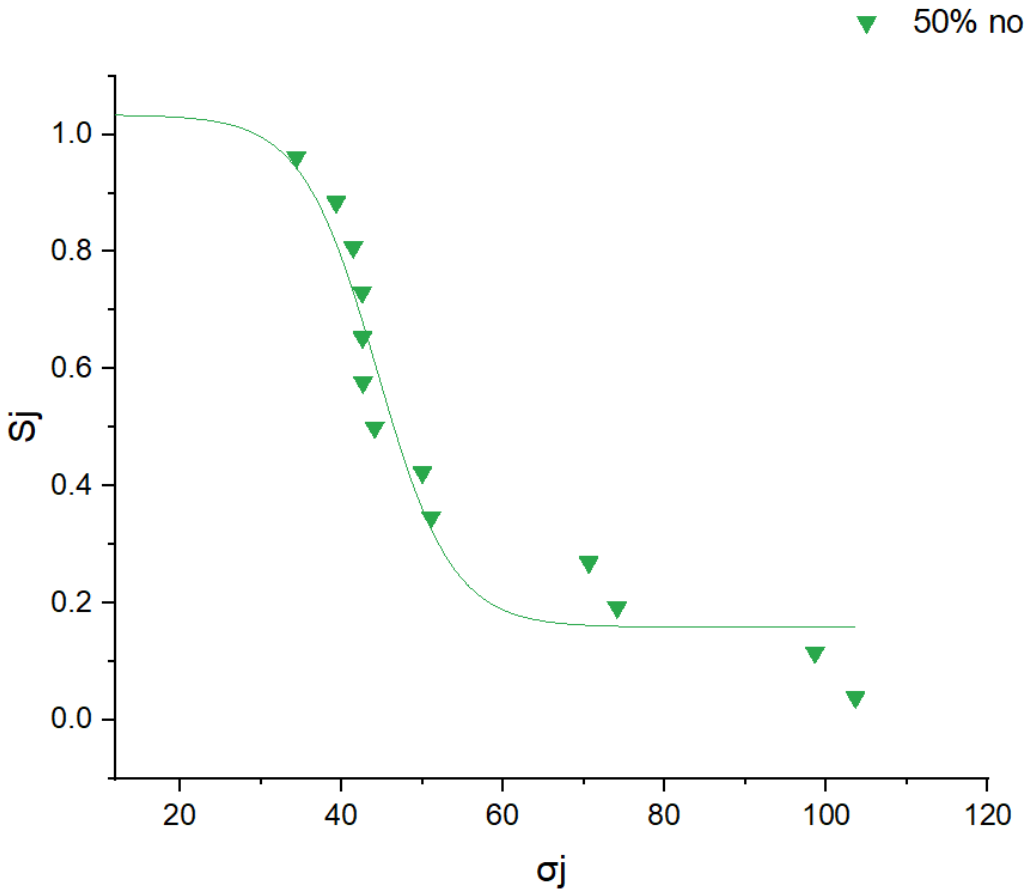

Figure 4.23: Weibull exponential fit only for the non heat treated samples.

j	d [mm]	h [mm]	σj [MPa]	Sj	lnσj	lnln(1/Sj)
1	14.82	5.81	0.62	0.96	-0.48	-3.24
2	14.87	5.69	1.67	0.88	0.51	-2.10
3	15.01	6.82	1.72	0.81	0.54	-1.54
4	15.01	6.51	1.80	0.73	0.58	-1.16
5	15.36	6.69	2.14	0.65	0.76	-0.86
6	15.21	5.99	2.18	0.58	0.78	-0.60
7	14.85	5.73	2.26	0.50	0.82	-0.37
8	15.65	6.02	2.41	0.42	0.88	-0.15
9	15.37	5.82	2.59	0.35	0.95	0.06
10	15.52	5.76	2.75	0.27	1.01	0.27
11	14.69	5.58	3.40	0.19	1.22	0.50
12	13.70	5.58	3.49	0.12	1.25	0.77
13	15.03	6.38	3.66	0.04	1.30	1.18

Table 4.2: wavy sinusoidal, heat treated.

j	d [mm]	h [mm]	σj [MPa]	Sj	lnσj	lnln(1/Sj)
1	14.99	5.18	2.94	0.96	1.08	-3.24
2	14.96	5.82	3.01	0.88	1.10	-2.10
3	14.78	5.10	3.16	0.81	1.15	-1.54
4	14.93	5.15	3.50	0.73	1.25	-1.16
5	15.04	5.78	3.69	0.65	1.32	-0.86
6	14.55	5.25	3.88	0.58	1.36	-0.60
7	15.11	4.94	4.02	0.50	1.39	-0.37
8	14.82	5.23	4.20	0.42	1.43	-0.15
9	14.84	5.87	5.15	0.35	1.64	0.06
10	15.00	5.16	6.20	0.27	1.82	0.27
11	15.07	5.04	6.47	0.19	1.87	0.50
12	15.04	5.10	8.63	0.12	2.16	0.77
13	14.79	5.53	9.48	0.04	2.25	1.18

Table 4.3: 50% porosity straight lines, heat treated.

j	d [mm]	h [mm]	σj [MPa]	Sj	lnσj	lnln(1/Sj)
1	14.65	4.71	1.68	0.96	0.52	-3.24
2	14.41	4.14	1.77	0.88	0.57	-2.10
3	14.85	4.47	1.81	0.81	0.59	-1.54
4	14.68	4.53	1.83	0.73	0.60	-1.16
5	15.61	4.56	1.94	0.65	0.66	-0.86
6	14.72	4.62	2.11	0.58	0.75	-0.60
7	15.02	4.59	2.92	0.50	1.07	-0.37
8	15.35	4.63	3.22	0.42	1.17	-0.15
9	14.61	4.59	3.49	0.35	1.25	0.06
10	15.23	4.32	3.63	0.27	1.29	0.27
11	14.51	4.52	3.95	0.19	1.37	0.50
12	15.10	4.29	4.56	0.12	1.52	0.77
13	14.91	4.67	4.72	0.04	1.55	1.18

Table 4.4: 60% straight lines, heat treated.

j	d [mm]	h [mm]	σj [MPa]	Sj	lnσj	lnln(1/Sj)
1	15.92	5.08	34.39	0.96	3.54	-3.24
2	15.04	5.59	39.31	0.88	3.67	-2.10
3	15.25	5.58	41.44	0.81	3.72	-1.54
4	15.64	6.22	42.55	0.73	3.75	-1.16
5	15.69	5.41	42.59	0.65	3.75	-0.86
6	15.46	6.29	42.62	0.58	3.75	-0.60
7	15.37	5.09	44.08	0.50	3.77	-0.37
8	15.64	5.90	49.98	0.42	3.91	-0.15
9	15.26	5.97	51.09	0.35	3.93	0.06
10	15.28	5.72	70.59	0.27	4.26	0.27
11	15.39	5.59	74.12	0.19	4.31	0.50
12	15.35	5.49	98.59	0.12	4.59	0.77
13	15.36	5.99	103.62	0.04	4.64	1.18

Table 4.5: 50% straight lines, not heat treated.

4.4 Electron Dispersive X-ray Spectroscopy (EDS)

From figure 4.24 and 4.25 it's possible to observe that the main peaks are the one of S, O and Na, confirming the presence of only Na_2SO_4 in the samples. The Oxygen peak is slightly smaller in the thermally treated sample, this could be caused by the fact that during the heating treatment the small water residues found in the hydrated compounds completely evaporates.

By comparing the EDS maps it's possible to note a decrease in C when the sample is subjected to a heating treatment, this is due to the fact that during the thermal treatment most of the PVP is burned.

In figure 4.26 is shown the EDS maps for the 50/50 component with wavy sinusoidal geometry; it can be seen that since it was not thermally treated there is presence of C coming from the PVP, as for the other elements it can be seen that they are evenly distributed on the surface of the specimen. In the peaks it's possible to see Na, S and O which confirms the presence of $LiNaSO_4$.

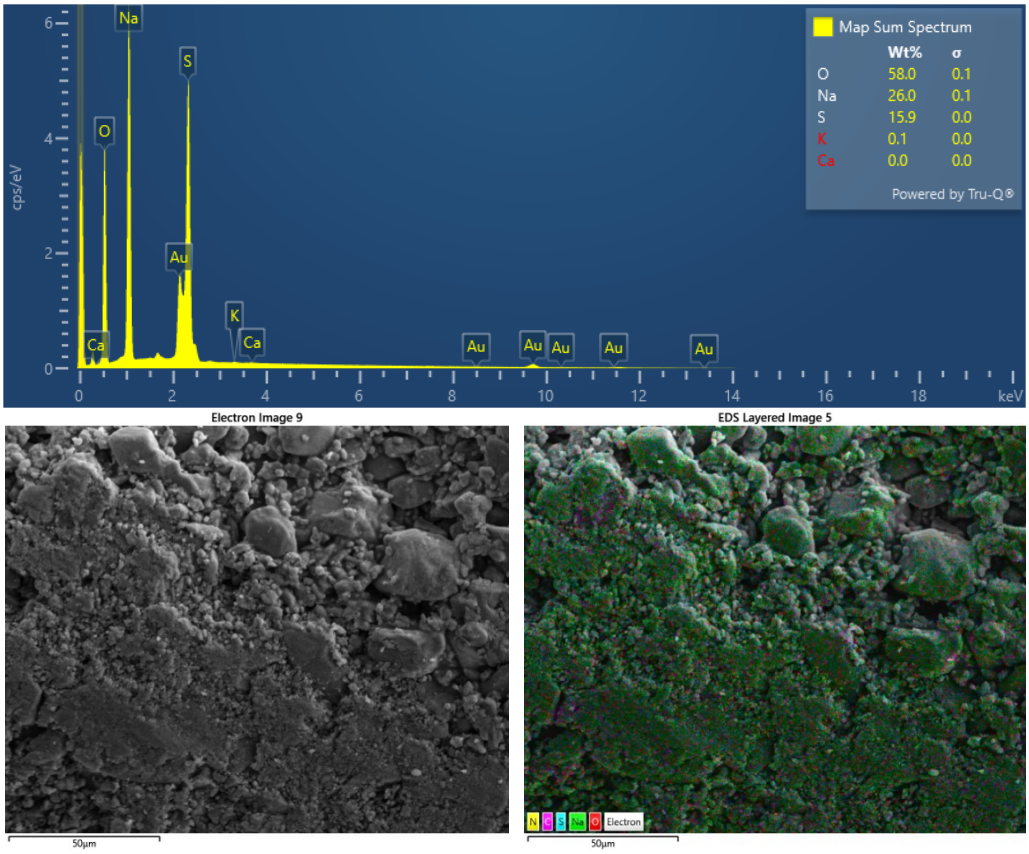

Figure 4.24: EDS of non thermally treated sample of Na_2SO_4.

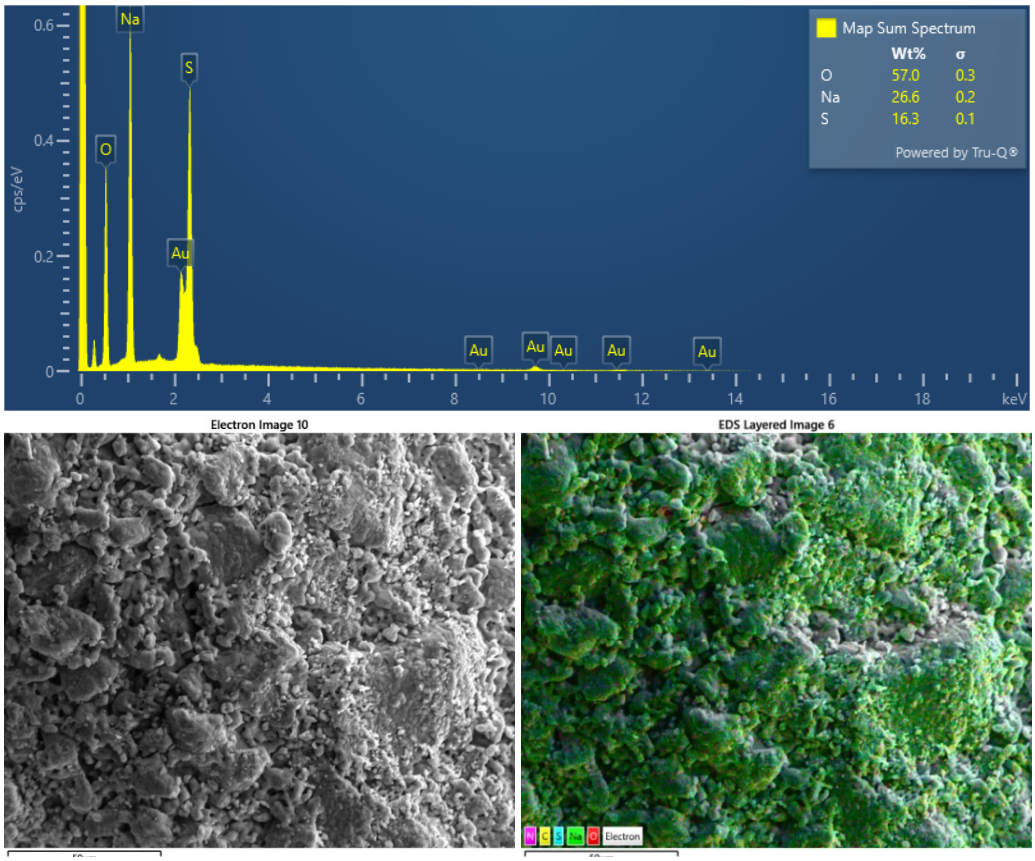

Figure 4.25: EDS of thermally treated sample of Na_2SO_4.

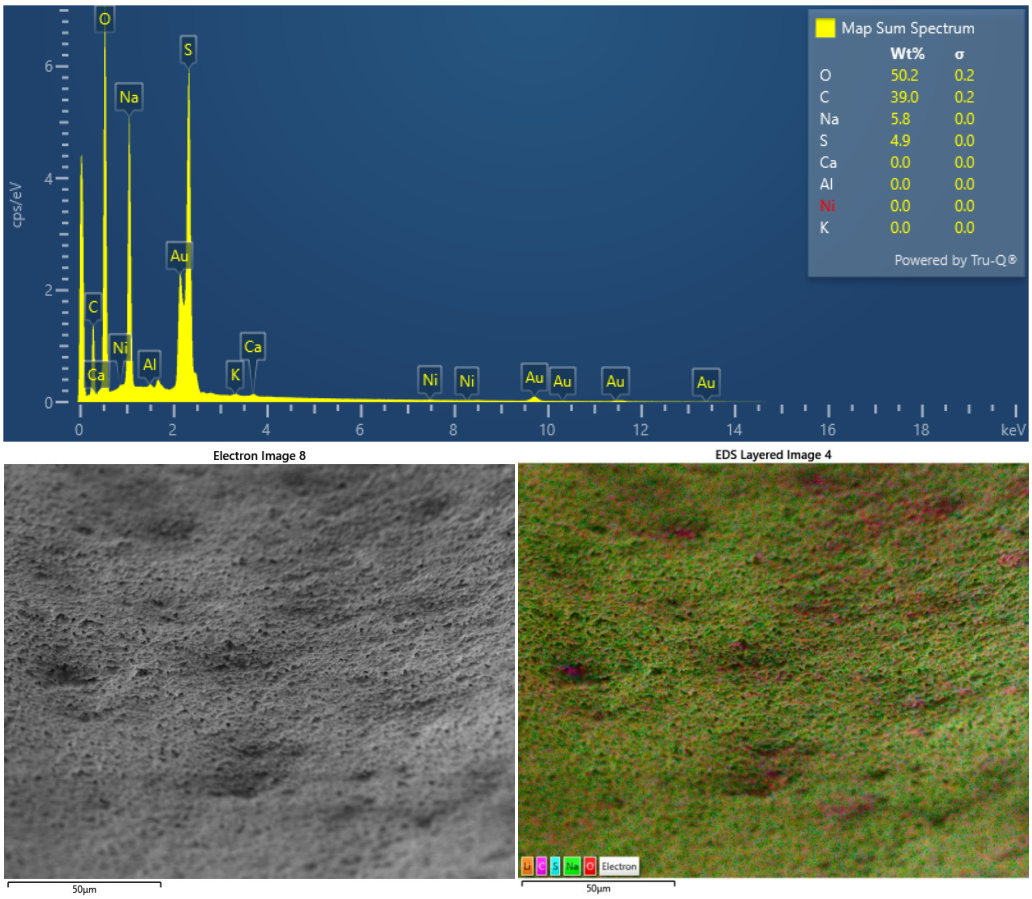

Figure 4.26: EDS of non thermally treated 50/50 wavy sinusoidal components.

4.5 Scanning Electron Microscopy (SEM)

In figure 4.27 the images with a 100x and 200x magnification shows that the printed filament is compact and homogeneous, meaning that during the printing phase the ink was kept at a constant pressure and that during the thermal treatment the variation in volume didn't cause any cracks or defects in the sample.

The images with 500x and 1500x magnification in figure 4.28 reveals a polycrystalline structure with well-defined grains. The grains exhibit a range of shapes, including irregular, angular, and rounded forms This suggests that the sample may have undergone some degree of sintering or recrystallization during the thermal treatment. The grains appear to be tightly packed with minimal porosity.

The grains are distributed relatively uniformly across the sample surface. There are no visible clusters or regions with significantly different grain sizes or orientations.

In conclusion it's possible to assess that the observed grain structure of the Na_2SO_4 sample has undergone some degree of sintering during the thermal treatment and the

presence of different grain shapes indicates that the sintering process may have been non-uniform, with some grains experiencing more significant growth than others.

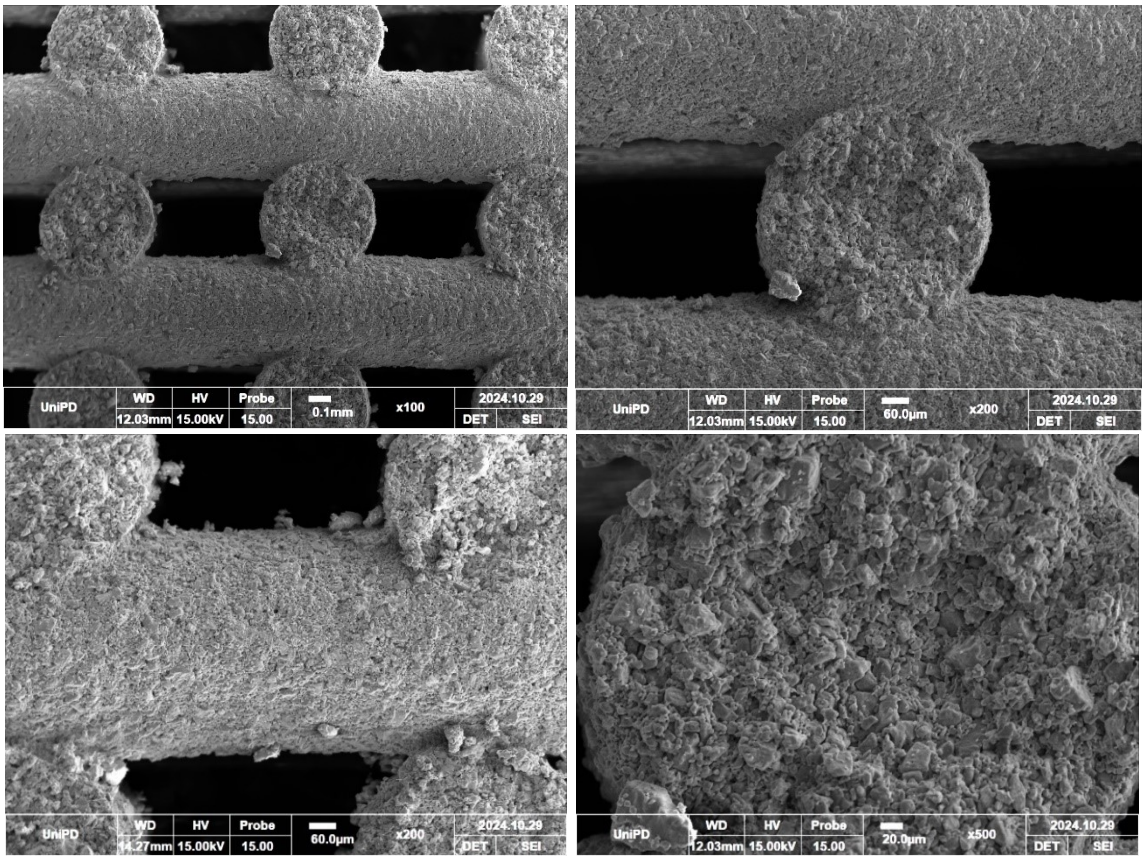

Figure 4.27: SEM images of heat treated Na_2SO_4 from top left to right: 100x, 200x, 200x, 500x,

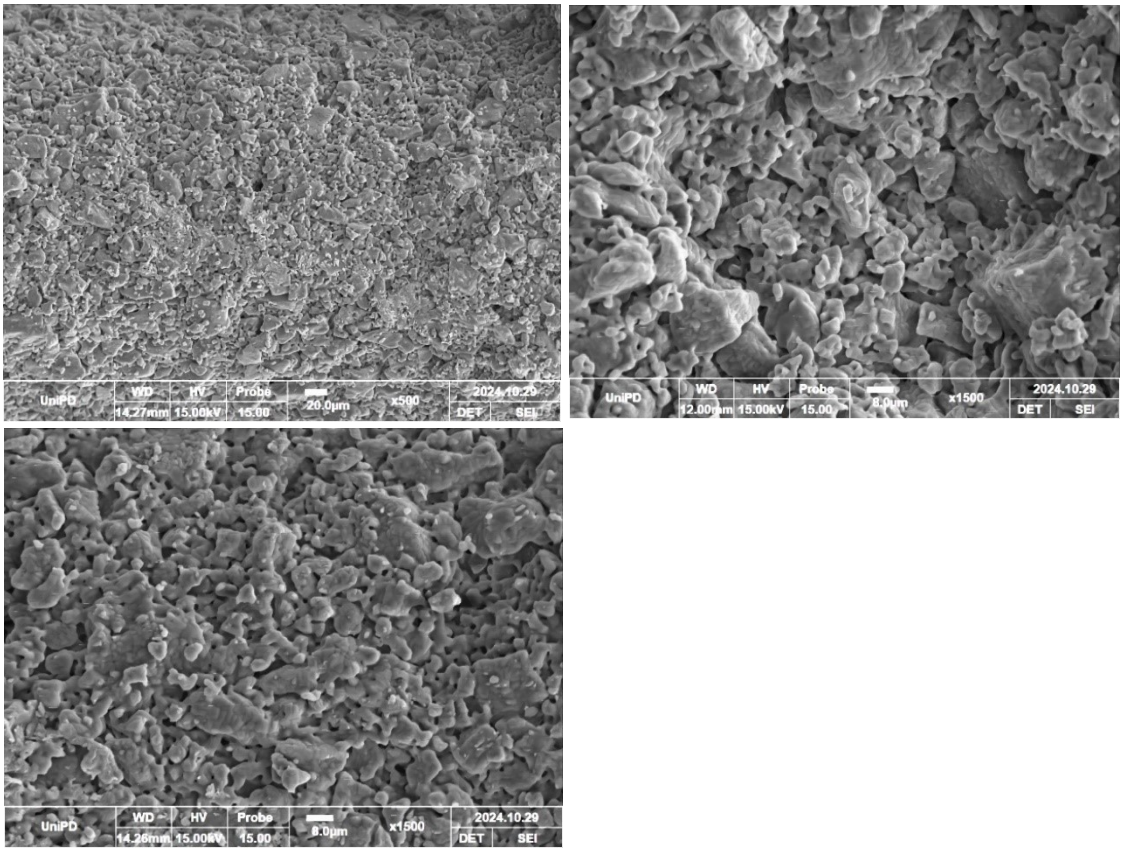

Figure 4.28: SEM images of heat treated Na_2SO_4 from top left to right: 500x, 1500x, 1500x.

The images with a 100x and 200x magnification in figure 4.28 shows a non perfectly homogeneous structure, some bigger grains can be detected along the filament. The filament is thicker compared to figure 4.27 because in the non heat treated samples PVP residues are still present.

The images with 1500x magnification of the non heat treated Na_2SO_4 samples (Figure 4.29) reveals a complex morphology with several distinct features; the sample appears to consist of agglomerated particles with varying sizes and shapes. These agglomerates likely formed during the drying and solidification of the printed specimen. Within the agglomerates, there are more pores and voids compared to the heat treated sample (Figure 4.28), this porosity could be attributed to the evaporation of the solvent (ethanol) during the drying process. The surface of the particles appears rough and uneven, with some regions exhibiting a more crystalline-like structure, this suggests that the Na_2SO_4 crystals may have begun to nucleate and grow during the drying process.

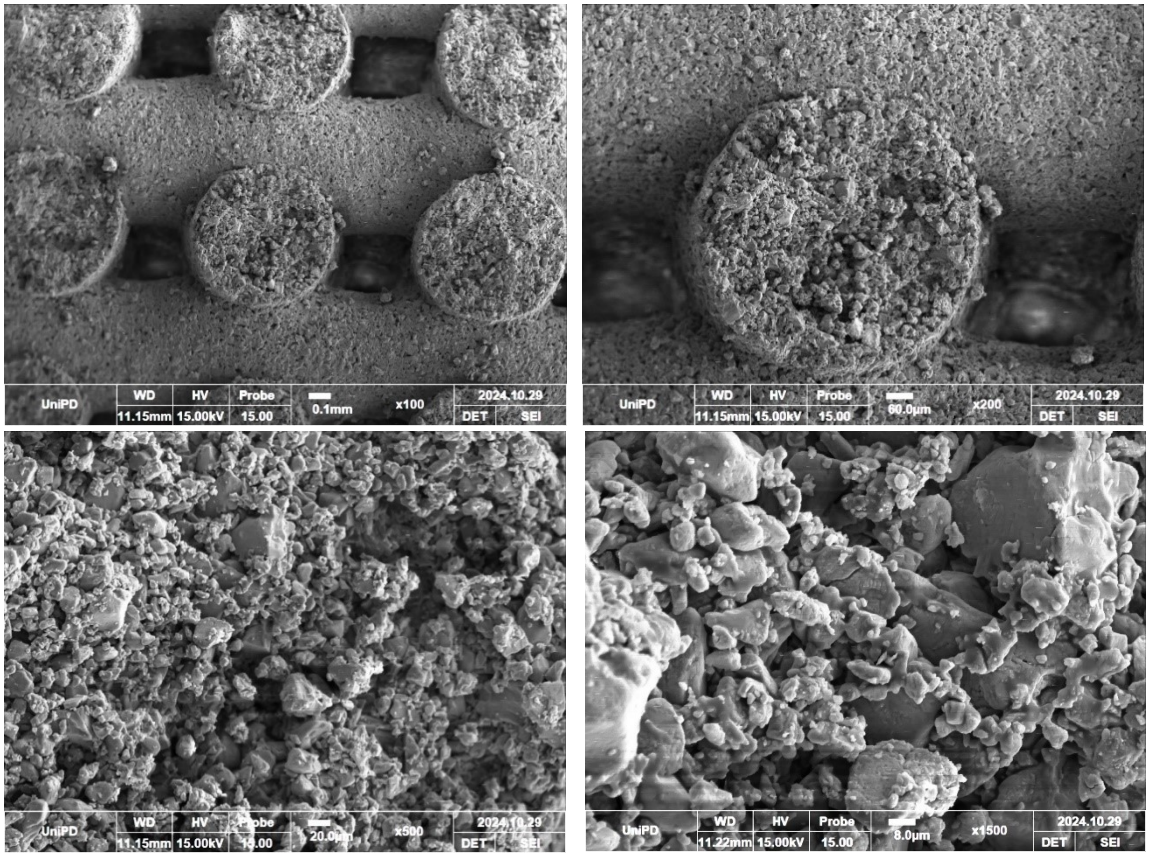

Figure 4.29: SEM images of non heat treated Na_2SO_4 from top left to right: 100x, 200x, 500x, 1500x.

For 50/50 molar components with wavy sinusoidal geometry it can be seen in figure 4.30 in the images with 200x and 500x magnification that the surface appears generally smooth for the exception of some small grains that may be due to the presence of the binder.

The 1500x magnification in Figure 4.31 shows a rough and grainy surface with small, irregularly shaped grains; looking at the section (last picture on the bottom) the images reveal a porous and non-uniform microstructure, unlike what could be observed for the 200x and 500x magnification ones. The particles are irregularly shaped and presence of pores and agglomerates can be detected which may be caused by the evaporation of ethanol during the drying phase.

The surface of the particles displays a heterogeneous morphology where more crystalline areas can be found, like in the previous case (Figure 4.29), this can be attributed to the fact that some crystals may have initiated a nucleation and growth process during the drying stage.

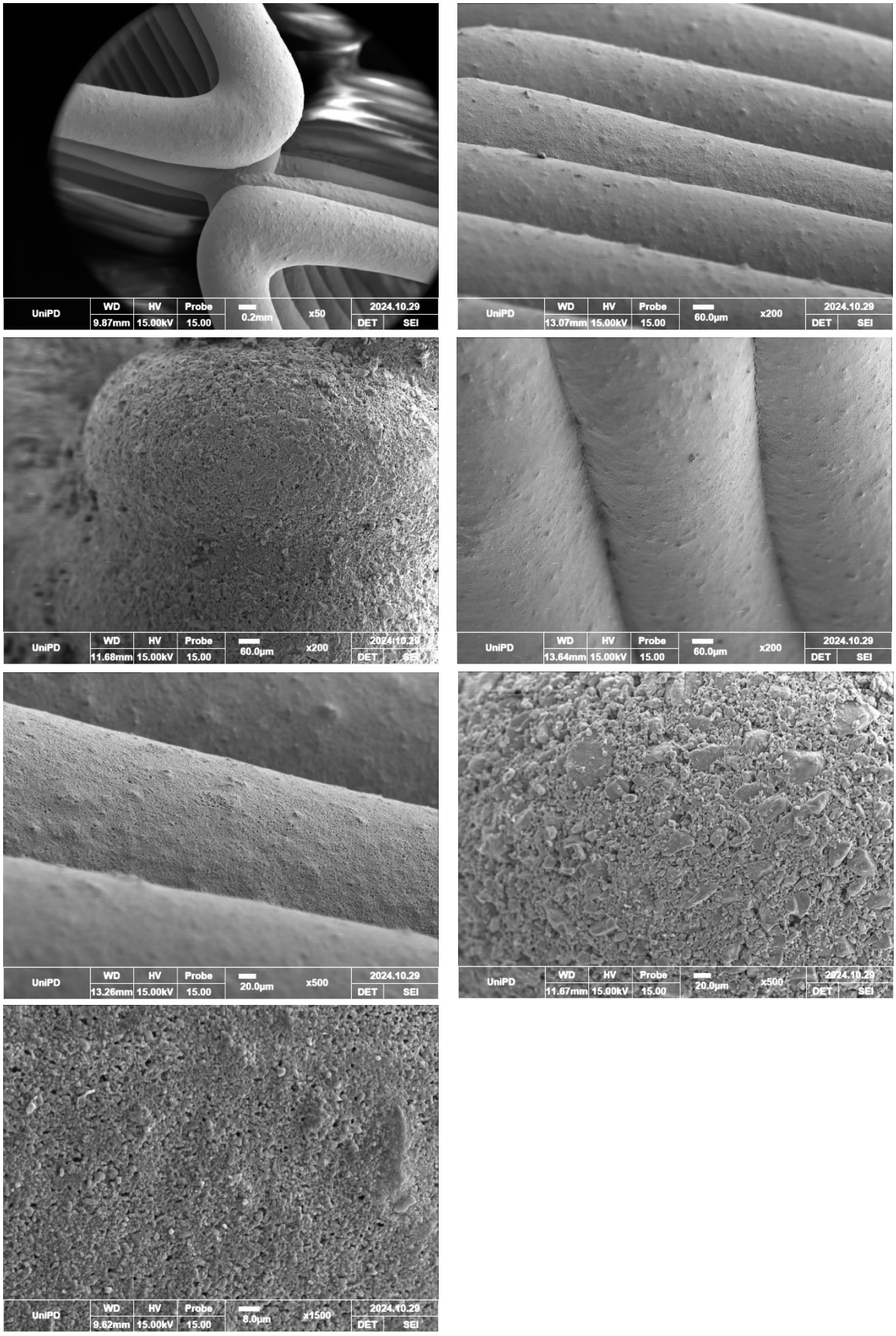

Figure 4.30: SEM images of 50/50 components with wavy sinusoidal geometry from left to right: 50x, 200x, 200x, 200x, 500x, 500x, 1500x.

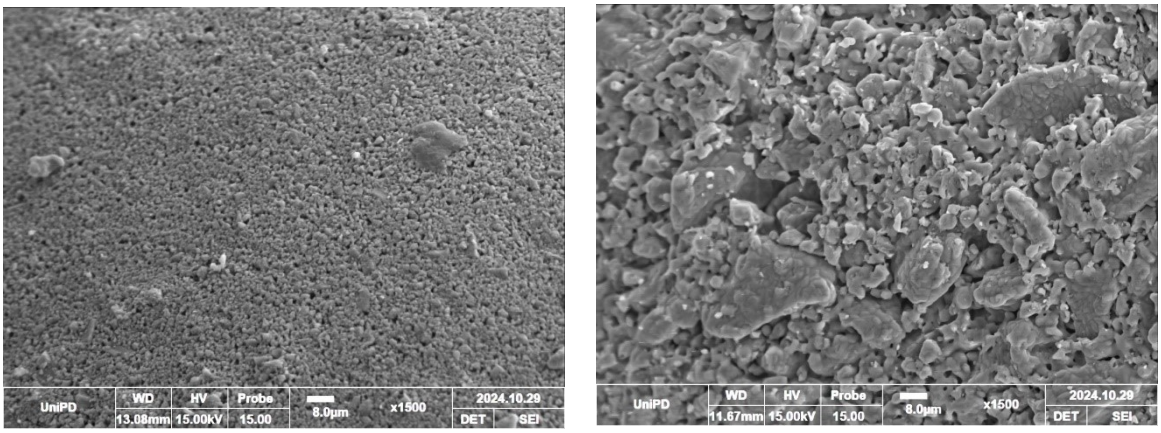

Figure 4.31: SEM images of 50/50 components with wavy sinusoidal geometry with 1500x magnification.

4.6 Thermal performances: DSC analysis

The thermal performances are assessed in terms of enthalpy of transition during heating and cooling DSC cycles, respectively ΔH_{trans} (h) and ΔH_{trans} (c) in table 4.6, and in terms of specific heat capacity, thermal diffusivity (α) and thermal conductivity (k).

For a PCM to be suitable for thermal energy storage applications it's important that in addition to having a high specific heat capacity or a high enthalpy of transition, a high thermal conductivity must be present in order to enhance the heat transfer efficiency.

3D structure samples	ΔH_{trans} (h) [J/g]	ΔH_{trans} (c) [J/g]	C_p [J/g°C]	α [mm²/s]	k [W/mK]
Na_2SO_4	46.7	47.4	1.159	0.25 ± 0.00 (24°C)	0.262 ± 0.001 (24°C)
Na_2SO_4 tt	47.7	49.1	1.190	-	-
Li_2SO_4	-	-	-	0.30 ± 0.01 (24°C)	0.265 ± 0.001 (24°C)
Li_2SO_4 tt	-	-	-	-	-
50/50	156.2	157.8	1.419	0.21 ± 0.01 (24°C)	0.206 ± 0.001 (24°C)
50/50 tt	163.6	163.1	1.561	-	-
79/21	179.0	179.9	1.895	0.24 ± 0.01 (24°C)	0.291 ± 0.001 (24°C)
79/21 tt	189.1	198.7	1.965	-	-

Table 4.6

In the table it's possible to observe how the values for the thermally treated components aren't too distant from the non thermally treated ones. The values of the enthalpy of transition are in agreement with the theory as well as the specific heat capacity and the thermal conductivity [13].

Chapter 5 – Conclusions

The aim of the work was to create a printable ink and design different type of geometries in order to print Na_2SO_4 structured components by direct ink writing. Tables with different Na_2SO_4 and Li_2SO_4 composition were made and thermally treated in order to inspect the correctness of the phase diagram and to study the colour variation of the samples containing Na_2SO_4.

From the analysis of the samples it can be said that:

- When subjected to heating treatments above 500°C the tablets containing Na_2SO_4 becomes darker in colour, this is probably due to the fact that Na_2SO_4 acts as a liquid phase that seeps into the spaces between particles, breaking down the bonds holding them together and allowing them to rearrange. This accelerated sintering process can result in larger, irregularly shaped particles and in a deterioration of the colour quality in the 79/21 and 50/50 samples, similarly to what happens when Na_2SO_4 is added to TiO_2.
- The printed geometries showed quite similar Weibull modulus compared to traditional ceramics. The fracture stress detected was highest for the non thermally treated 50% porosity samples (m = 2.95) and lowest for the wavy sinusoidal thermally treated sample (m = 2.56).
- The XRD analysis for both the tablets and the printed components showed that the thermal treatment performed was effective in removing the binder (polyvinylpyrrolidone) and the hydrated compounds. In the case of the tablets it was useful to asses the correctness of the phase diagram, which was confirmed.
- SEM images showed compact and homogeneous structures when the components were heat treated while a more porous and irregular structure was found in the non heat treated components.
- The thermal analysis revealed that the heat storage capacity is preserved in the components after being thermally treated.

Bibliography

[1] M. I. Lone, R. Jilte, 2020, A review on phase change materials for different applications, *Materials today: proceedings,* 46 (20): 10980-10986.

[2] L. Zhou, J. Miller, J. Vezza, M. Mayster, M. Raffay, Q. Justice, Z. Al Tamimi, G. Hansotte, L. D. Sunkara, J. Bernat, Additive Manufacturing: A Comprehensive Review, 2024, *Sensors,* 24: 2668.

[3] M. Saadi, A. Maguire, N. T. Pottackal, M. S. H. Thakur, M. M. Ikram, A. J. Hart, P. M. Ajayan, M. M. Rahman, 2022, Direct ink writing: a 3d printing technology for diverse materials, *Advanced Materials*, 34(28):2108855.

[4] S. Doppiu, J. L. Dauvergne, A. Serrano, E. Palomo del Barrio, 2019, The Li_2SO_4–Na_2SO_4 system for thermal energy storage. Materials, 12 (22): 3658.

[5] P. Patnaik, Handbook of inorganic chemicals, 2003, McGraw-Hill.

[6] Y. C. Venhudar, L. Iyengar, K. V: Krishna Rao, Phase transitions in sodium lithium sulphate, *Journal of material science*, 1985, 4: 1010-1013.

[7] G. Jauncey, The scattering of x-rays and Bragg's law, *Proceedings of the national academy of sciences*, 10(2):57‑60, 1924.

[8] M. Tiryakioglu, D. Hudak. Unbiased estimates of the Weibull parameters by the linear regression method, 2008, *Journal of materials science*, 43: 1914–1919.

[9] P. P. Fedorov, V. Y. Proydakova, S. V. Kuznetsov, V. V. Voronov, A. A. Pynenkov, K. N. Nishchev, Phase diagram of the Li2SO4–Na2SO4 system, 2019, *Journal of the American Ceramic Society,* DOI: 10.1111/jace.16996.

[10] Y. Wang, K. A. Mumford, S. Shen, Y. Li, Effect of low melting temperature salt (Na_2SO_4) addition on the phase transformation, crystal growth, and chroma of titanium dioxide pigments, *Powder Technology,* 2015, 284: 204-209.

[11] R. Danzer1, T. Lube, P. Supancic, Fracture statistics of ceramics – a short overview, *11th International Conference on Fracture*, Turin, Italy.

[12] S. Guo, R. Liu, X. Jiang, Statistical Analysis on the Mechanical Properties of Magnesium Alloys, 2017, *Materials*, 10:1271.

[13] A. Bayon, M. Liu, D. Sergeev, M. Grigore, F. Bruno, M Muller, Novel solid–solid phase-change cascade systems for high-temperature thermal energy storage, 2019, *Solar Energy,* 177: 274-283.